FINAL REPORT

Useful Prediction of Climate Extreme Risk for Texas-Oklahoma at 4-6 Years

SERDP Project RC-2709

AUGUST 2018

Dr. Simon Shih-Yu Wang
Utah State University

SERDP
DOD ▪ EPA ▪ DOE

Page Intentionally Left Blank

REPORT DOCUMENTATION PAGE	*Form Approved* *OMB No. 0704-0188*

1. REPORT DATE *(DD-MM-YYYY)*	2. REPORT TYPE	3. DATES COVERED *(From - To)*
08/15/2018	SERDP Final Report	03/16/2017 - 08/15/2018

4. TITLE AND SUBTITLE Useful Prediction of Climate Extreme Risk for Texas-Oklahoma at 4-6 Years	**5a. CONTRACT NUMBER** W912HQ-17-P-0013
	5b. GRANT NUMBER
	5c. PROGRAM ELEMENT NUMBER
6. AUTHOR(S) Simon Shih-Yu Wang	**5d. PROJECT NUMBER** RC-2709
	5e. TASK NUMBER
	5f. WORK UNIT NUMBER
7. PERFORMING ORGANIZATION NAME(S) AND ADDRESS(ES) Utah State University 4820 Old Main Hill Logan, UT 84322-4820	**8. PERFORMING ORGANIZATION REPORT NUMBER** RC-2709
9. SPONSORING/MONITORING AGENCY NAME(S) AND ADDRESS(ES) Strategic Environmental Research and Development Program 4800 Mark Center Drive, Suite 16F16 Alexandria, VA 22350-3605	**10. SPONSOR/MONITOR'S ACRONYM(S)** SERDP
	11. SPONSOR/MONITOR'S REPORT NUMBER(S) RC-2709

12. DISTRIBUTION/AVAILABILITY STATEMENT
Distribution A; unlimited public release

13. SUPPLEMENTARY NOTES

14. ABSTRACT
This project tackles the challenge for predicting water-cycle extremes in Texas and Oklahoma as severe as the 2015 and 2016 floods beyond seasonal timescale. The project’s main objectives were (i) tracking the 4-6-year ENSO (El Niño-Southern Oscillation) and teleconnections and (ii) characterizing uncertainty in the 4-6-year prediction, testing the hypothesis that predictability within the reportedly strengthened 4-6-year ENSO cycle and its teleconnection can be extracted to provide extended outlook for extreme flood risk.

15. SUBJECT TERMS
floods, flooding, El Nino, ENSO, teleconnection, flooding prediction, flood risk, Community Earth System Model, CESM, Large Ensemble Project, Coupled Model Intercomparison Project, CMIP, climate models, hurricanes, Hurricane Harvey, Texas, Oklahoma

16. SECURITY CLASSIFICATION OF:			17. LIMITATION OF ABSTRACT	18. NUMBER OF PAGES	19a. NAME OF RESPONSIBLE PERSON
a. REPORT	b. ABSTRACT	c. THIS PAGE			Simon Shih-Yu Wang
					19b. TELEPHONE NUMBER *(Include area code)*
UNCLASS	UNCLASS	UNCLASS	UNCLASS	61	435-757-3121

Standard Form 298 (Rev. 8/98)
Prescribed by ANSI Std. Z39.18

Page Intentionally Left Blank

Page Intentionally Left Blank

Table of Contents

Acknowledgement

The Principal Investigator acknowledges the contributions from the following graduate student and professional staff within the Department of Plants, Soils and Climate, as well as collaborator in research that have made contributions to this project:

Dr. Boniface Fosu, Ph.D. candidate (degree awarded in 2018)
Mr. Adrián Tábara, Programmer
Dr. Jin-Ho Yoon, Associate Professor of Gwangju Institute of Science and Technology, ROK
Dr. Ming-Hui Lo, Associate Professor of National Taiwan University, Taipei, TW

The Principal Investigator is grateful to Dr. Kurt Preston, the Program Manager for Resource Conservation and Climate Change, Ms. Stephanie Lawless and Ms. Macrina Xavier for their continued thoughtful guidance and feedback throughout the project.

List of Figures

List of Acronyms

CESM:	Community Earth System Model
CMIP5:	Coupled Model Intercomparison Project Phase 5
DoD:	Department of Defense
ENSO:	El Niño-Southern Oscillation
ERSST:	Extended Reconstructed Sea Surface Temperature version 5 or v5
LEP:	Large Ensemble Project
MJO:	Madden Julian Oscillation
PMM:	Pacific Meridional Mode
QDO:	Quasi-Decadal Oscillation
SST:	Sea surface temperature
WNP:	Western North Pacific
CLIVAR:	Climate Variability and Predictability

Keywords

Two-Year Prediction; Extreme Events; Climate Variability; Texas and Oklahoma; DoD Installations; ENSO; Large Ensemble Simulation

Abstract

Objectives: This limited-scope project tackles the challenge for predicting water-cycle extremes in Texas and Oklahoma as severe as the 2015 and 2016 floods beyond seasonal timescale. The impact of extreme floods during spring and the hurricane season on Department of Defense (DoD) facilities has elevated, straining infrastructural limits and operational capability. The project's main objectives are (i) tracking the 4-6-year ENSO (El Niño-Southern Oscillation) and teleconnections and (ii) characterizing uncertainty in the 4-6-year prediction, testing the hypothesis that predictability within the reportedly strengthened 4-6-year ENSO cycle and its teleconnection can be extracted to provide extended outlook for extreme flood risk.

Technical Approach: We utilized long simulations produced by the Community Earth System Model (CESM) of the Large Ensemble Project (LEP) and observational data sets. Diagnostics of the LEP simulations of the 4-6-year ENSO cycle and its precursor patterns across the three major oceans were conducted to examine the evolution and regional impacts. Furthermore, an add-on analysis for Hurricane Harvey in the context of climate attribution and implication to prediction was performed. The guiding principle here is to understand the differing synoptic processes embedded in the large-scale variability. Extremely wet and dry seasons in Texas and Oklahoma were objectively identified within a global reanalysis, the CESM, and the suite of climate models from the Coupled Model Intercomparison Project (CMIP), and their connection with ENSO was evaluated. The synoptic elements that could either produce consecutive rainstorms or stall a tropical storm were investigated in the model projections, to assess their role in the prediction uncertainty.

Results: The LEP simulations reveal stabile signal in the 4-6-year ENSO cycle with an amplified signal after 2010, suggesting increased predictability in the future, warmer climate. While both excessive precipitation and intense drought in Texas are projected to increase towards 2050, their association with the energized 4-6-year ENSO mode will likely strengthen and become increasingly predictable. However, groundwater storage in Texas and Oklahoma will likely decrease due to diminishing recharge caused by concurrent increases in drought, which offsets the effect of added rains. A greater implication of these results is that the alternation between excessive wet years and severe drought years will amplify. Prediction of ENSO impacts could be improved by capturing the western and north Pacific precursors showing strong air-sea interactions a year before a mature ENSO phase develops. These variations are manifest in the advection process of the sea surface heat budget, which acts in concert with the air-sea heat fluxes to foster ENSO development. However, these processes were compounded in the December 2015 Missouri flood, as the El Niño teleconnection interfered with the Madden Julian Oscillation, which contributes to uncertainty. Finally, through the analysis of Hurricane Harvey, we found that the stalling characteristics of tropical storms will enhance moderately, but prediction of hurricanes beyond a season is not feasible due to the lack of ENSO connection.

Benefits: A physically based approach to anticipating extreme floods in Texas and Oklahoma was developed within this limited-scope project, one that could be straightforwardly adapted for other states and international bases. Project result implies an impending drought in 2018 and potential risk of widespread flood in 2019, along with a long-term outlook for water resources

planning. Additionally, a mesoscale modeling approach adds value to quantifying extreme weather threat around Texas and Oklahoma, where precipitation is becoming more intense. Model data and forecast information generated within this project are made available through a public university's webserver, to be widely available for DoD and civilian use.

1. Objectives

This research project was developed in responding to RCSEED-17-01 call for proof of concept (2015), to target two of the five RCSEED Research Needs: *modes of climate variability* (#2) and *using recent historical signals to update the non-stationarity of the climate signal* (#4). After a year of execution, the project has yielded proof-of-concept results from analyzing the precursor of persistent weather patterns forced by traceable oceanic and atmospheric signals.

The first objective of this project is *Tracking the 4-6-year ENSO mode and teleconnections.* Previous studies including those by the PI[4,5] have linked an increasingly energetic 4-6-year frequency of El Niño-Southern Oscillation (ENSO) with a global propagation pattern in both the atmosphere and the oceans. It is hypothesized that a diagnostics-based analysis can extract the extended predictability embedded within the full cycle of this energized 4-6-year ENSO frequency, as well as its teleconnection impacts on Texas.

Our second objective targets *Characterizing uncertainty in the 4-6-year prediction.* The uncertainty of long-range prediction for ENSO and its impacts on regional hydrologic cycle is challenged by the inability of coupled models in simulating the proper ENSO frequency. Being able to diagnose model performance of this emerging type of ENSO and its various precursors will help characterize uncertainty when it comes to predicting the teleconnection pattern at different lifecycle of ENSO. Uncertainty associated with random weather disturbances (like Hurricane Harvey) also requires investigation in the projection of extreme precipitation.

2. Background

This research was stimulated by the extreme flood in Texas during spring 2015, one of the many floods resulted from record rainfall produced by consecutive storms. On the climate forcing, the 2015 event was linked to the combined effects of El Niño and Arctic variability, and events like that can potentially be forecast beyond seasonal time scale. By contrast, the case of hurricane Harvey represents stochastic weather perturbations that can hardly be forecast more than a week ahead, but its climate drivers did show traceable climate change signals and are investigated as well. The extent to which the current climate projection practice handles these two similarly devastating yet dynamically different deluge events, and what it means for DoD installation management, has not been addressed.

The DoD operates many installations in Texas and Oklahoma and these states had seen several high-impact extreme events: Record drought in 2011 followed by 2015-16 floods, and Hurricane Harvey in 2017, causing severe damages and logistic problems in those installation sites. These extreme events led the National Guard to mobilize various aircraft with a full extent of personnel and engineer units to assist in logistical support and rescue. While some of the synoptic/climatic processes of such extreme precipitation could be predicted beyond weather timeframe, some are theoretically impossible to forecast. As shown in Fig. 1 (left), the May 2015 Texas flood resulted from a long-standing atmospheric "trough" channeling waves of rainstorms toward Texas (red arrow). By contrast, Hurricane Harvey devastated Texas under a weak atmospheric pattern (Fig. 1 right). While long-term prediction of such tropical storms is difficult, their change in the projected climate scenarios and implication were investigated.

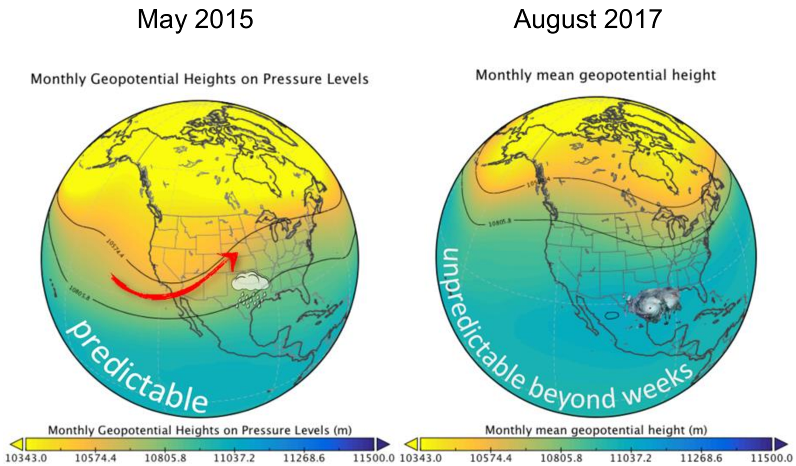

← Fig. 1 (left) Ocean and atmosphere-forced flooding in May 2015 associated with a standing upper-level trough creating month-long heavy rains, versus (right) an upper-ridge or "fair weather" condition in which Hurricane Harvey was stalled over Texas in August 2017 producing consecutive days of extreme rainfall. [Author generated figures]

Observational and modeling evidence suggests the existence of a prolonged, circum-global propagation in tropical oceanic and atmospheric variables accompanying the ENSO evolution[3]. Most studies focusing on the evolution and predictability of ENSO stressed the surface wind forcing and temperature anomalies up to two seasons in advance, but few explored the propagation features embedded in the energetic 4-6-year lifecycle of ENSO. Even though ENSO evolution and precursors have been studied extensively[6], the newly identified circumglobal propagations associated with ENSO could lend support to the development of long-term prediction beyond seasonal timescale. This aspect was examined in this project.

Before Hurricane Harvey hit the U.S. state of Texas in August 2017, heavy precipitation events of non-hurricane origins have already caused multiple floods since April 2015 with devastating consequences. The May 2015 flood resulted from over 400 mm above-normal rainfall falling on Texas and, subsequently, the May 2016 flood took 12 lives and caused historic river levels, making it the fifth major flood event and the second 500-year flood in the Houston area. The synoptic conditions associated with the spring floods in 2015 and 2016 are not too distinct from each other, both featuring a quasi-stationary trough west of the southern Great Plains generating short waves and squall lines[1]. The developing El Niño in May 2015 further deepened this quasi-stationary trough while enhancing the low-level jet[4]. Global warming acted to strengthen the El Niño teleconnection[7,8] that affects the southern Great Plains. Hurricanes such as Harvey produce excessive rainfall and have led to flood, but such weather systems are random in nature and linking them to large-scale forcing is difficult[9].

The recent succession of floods in Texas could lead to oversight of the risk in severe drought. Not too long ago in 2011, Texas underwent the worst 1-year drought on record[10] with unprecedented heat waves[11]. Both the strong La Niña and anthropogenic warming played a role in the severity and increased probability of this drought[12], an opposite pattern of the El Niño-enhanced 2015 flood. In late 2017, the NOAA Climate Prediction Center (CPC) indicated a 70% chance for a La Niña to develop through February 2018, prompting an anticipation of a drought to develop over the Texas region. This project published a paper in early 2018[1] about a possible "comeback" of drought near Texas and the most recent (August 2018) Palmer Drought Severity Index as shown in Fig. 2 does verify the emergence of drought. This result implies a short-term climate prediction in the face of recent La Niña and a longer-term outlook for water resources planning. Thus, we decided to evaluate climate model predictions of Texas' water cycle extremes represented by excessive wet spring and severely dry summer and associated impact on groundwater.

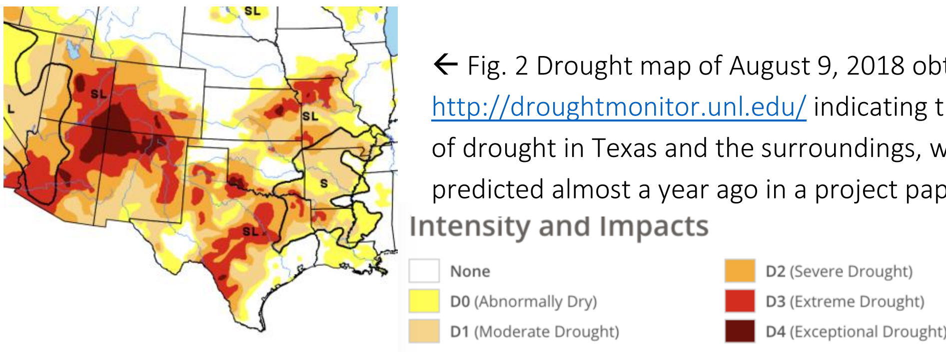

← Fig. 2 Drought map of August 9, 2018 obtained from http://droughtmonitor.unl.edu/ indicating the emergence of drought in Texas and the surroundings, which was predicted almost a year ago in a project paper[1].

3. Materials and Methods

Earlier climate models are primarily biased with a pronounced biennial frequency and most fail to produce the observed propagation features, either local or global[13,14]. Pilot study of this project has identified a few newer models that are capable of simulating the propagating evolution of ENSO[3]. One of the good performers is the Community Earth System Model (CESM) and it also simulates well the ENSO teleconnection impact on Texas[1,4]. Thus, CESM was chosen to be the modeling tool of this project.

We utilized large ensembles of long runs produced by the National Center for Atmospheric Research (NCAR) using the CESM v1[15], given its published performance on the ENSO frequency and teleconnection over North America[4,16]. The CESM Large Ensemble Project (LEP) was designed for studying internal climate variability and climate change. The stability of the 4-6-year ENSO cycle and associated impacts on Texas and vicinity have been examined in these simulations[1,17]. Modern-era global reanalysis data and other data sets including the Extended Reconstructed Sea Surface Temperature (ERSST v5) and NOAA's Precipitation Reconstruction over Land and over ocean were used. The LEP produced wo periods of data: 1920-2005 with all external forcing and 2006-2080 with RCP8.5 forcing (the range of radiative forcing increase at 8.5 W/m^2 per year till the year 2100 relative to pre-industrial values). To provide a baseline performance measure and for attribution analysis, we also included 17 models from the Coupled Model Intercomparison Project Phase 5 (CMIP5) historical single-forcing experiments. Other observational data sources include the NCEP/NCAR Reanalysis starting in 1948[18] in order to analyze interdecadal changes. Other datasets include the Extended

Reconstructed Sea Surface Temperature (ERSST, v3b) derived from the International Comprehensive Ocean–Atmosphere Dataset[19] for the ENSO indexing, and the NOAA Precipitation Reconstruction over Land (PREC/L) gridded product of 0.5° degree resolution[20].

To quantify uncertainty in the projection of near-future ENSO teleconnection and impacts on Texas, we compared the monthly Niño-3.4 index with mean precipitation and frequency of extreme precipitation for different periods. All data within either period was detrended to minimize the effect of any interdecadal cycle or forced trend. Additional analysis was performed using the CESM LEP for different time slices in order to gauge uncertainty range while examining the effect of global warming on regional climate response.

4. Results and Discussion

Project results demonstrate potential predictability of the water cycle extremes in Texas and Oklahoma at long (> 2 years) lead time, through the pathway of a projected strengthening in the link with the 4-6-year ENSO mode. A webpage was developed to provide preliminary prediction information of extreme flood risk in Texas, out to three years (2018-2020).

a. Extreme water cycles: deluge vs. drought

In terms of climatology, CESM-LE captured the spring rainy season but underestimates the secondary rainfall peak in fall. Overall, precipitation in Texas and Oklahoma is projected to increase throughout the year with a larger increase in spring (April-June), in which the increased precipitation amounts to 15-20% by the end of 21st century[1]. Subsequently, we examine the El Niño impact on Texas' spring precipitation based upon the precipitation composites. The analysis during 1950-1995 (Fig. 3a) shows anomalous precipitation over southeastern Texas and part of Oklahoma and Louisiana. In the near-future simulations (Fig. 3c) and the historical simulations (Fig. 3b), there is a marked increase in the ensemble mean precipitation composite difference between El Niño and La Niña in Texas and Oklahoma. In terms of the changing teleconnection associated with ENSO, Figs. 3e and 3f show the CESM-LE geopotential height differences at 250 hPa; these are generally in agreement with the observed pattern in Fig. 3d including the synoptic trough west of Texas. The El Niño-enhanced low-pressure anomaly west of Texas is increased by about 35% during 2010-2060 under the climate warming (Fig. 3f), while the broad-scale teleconnection pattern remains similar to the historical simulations (Fig. 3e).

By examining the sliding correlation between spring precipitation anomalies in Texas and the ENSO cycle from the observation and CESM LEP data (not shown), we found a clear decadal-scale fluctuation in the observation with a more pronounced increase after year 2000. The CESM produces a gradual increase and it becomes persistently significant after 2000 at the 95% level. These results echo the observation that Texas' spring precipitation response to the ENSO evolution has intensified and this trend is projected to continue. A greater implication is that the alternation between excessive wet years and severe drought years will amplify and, as our following analysis will shows, such an alternation between flood and drought atmospheric precursors is potentially predictable.

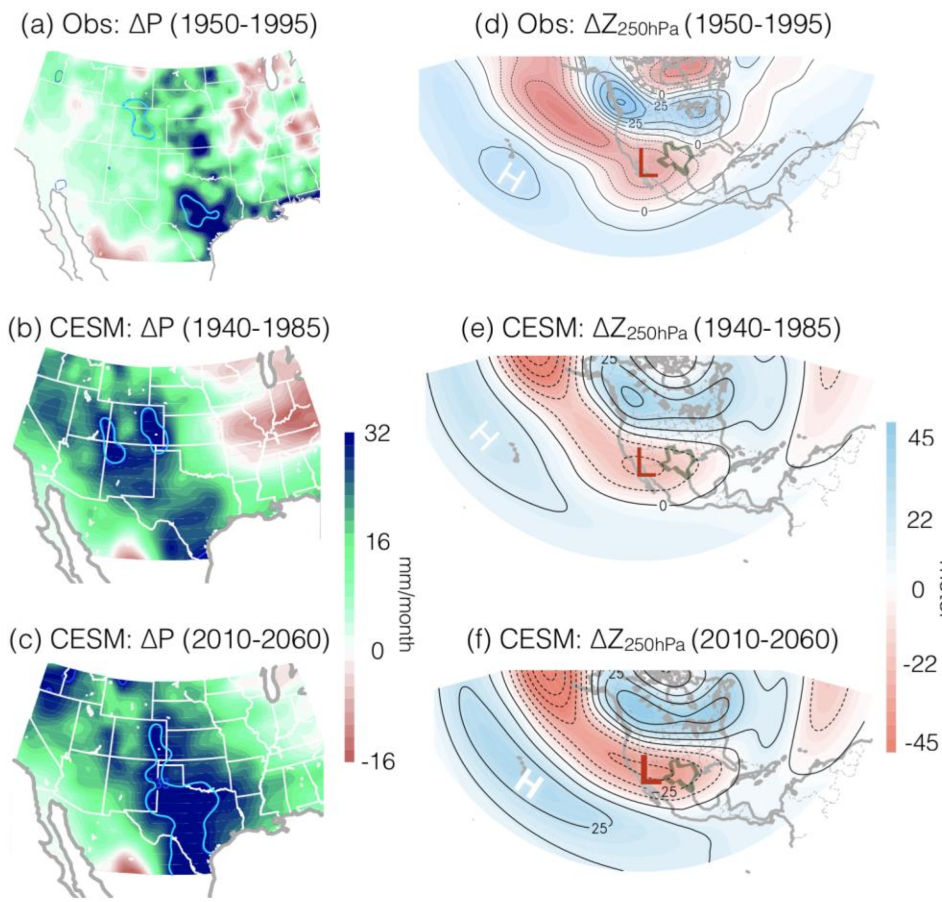

↑Fig. 3 Precipitation differences (ΔP) between the El Nino and La Nina composites (see text) during the April-June seasons of (a) 1950-1995 from the observation data and the CESM-LE ensemble mean during (b) 1940-1985 and (c) 2010-2060; blue contours outline the significance level of p<.001. (d)-(f) Similar to (a)-(c) but for the 250hPa geopotential height difference (ΔZ) from reanalysis and CESM-LE data for the same periods. The letter L indicates low-pressure anomaly centers and H indicates high pressure. [Figure adopted from the project publication of Yoon et al.[1]]

To quantify the effect of the changing ENSO teleconnection on the extreme wet/dry spring and summer in the SGP, we computed the frequencies of (a) back-to-back wet springs consisting of spring precipitation anomalies greater than 1 standard deviation occurring in two consecutive years, (b) same as (a) but only for those occurring with an El Niño winter in between, and (c) reversal of (b) for consecutive two dry summers with the JAS precipitation deficits occurring with a La Niña winter in between. In the observation, the period of 1985-2015 exhibits a distinctly higher frequency in all three cases than the earlier 30 years. Meanwhile, the CESM-LE projects an almost linear increase in both the El Niño associated wet springs[4] and the La Niña accompanied dry summers toward the end of the 21st century[1].

The effect on groundwater storage resulting from the aforementioned concurrent increase in drier summers was also examined. Based upon CESM LE's groundwater recharge and infiltration outputs, together with other surface variables that comprise the terrestrial water budget, the trends of the 2006-2100 period were computed. The simulated groundwater storage anomalies (Fig. 4) indicate a significant decrease with a rete of -2.3 cm/decade in the future, with most ensemble members falling below zero after 2040. This particular analysis shows that the decline in the recharge rate is profound as the recharge will have become deficit after 2020. While an increase in annual precipitation is projected in Texas, surface evapotranspiration plays a substantial role in affecting the terrestrial water budget. We show that the increased rate of evapotranspiration exceeds the rate of precipitation minus surface runoff, leading to a smaller infiltration and this reduces the groundwater recharge and soil water, amounting to a significant decrease with a rate of approximately -1.5 cm per decade in the future[1]. This result has implication to the design and maintenance of military installations that rely on groundwater resource, an information that is additional to coping with flood risk.

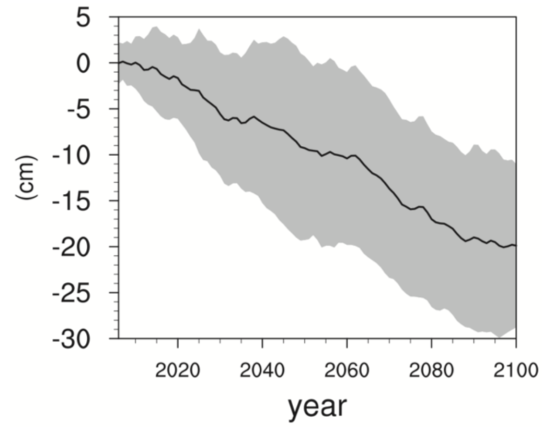

Fig. 4 CESM LE's groundwater storage anomalies over Texas relative to 2006 values in the ensemble mean (line) and model spread (shading). [from Yoon et al.[1]]

b. Synoptic processes of extremes rainfall "cases" associated with ENSO

In the same year of the 2015 Texas flood, three days of extreme rainfall in the middle of the Mississippi River during late December led to massive winter flooding in Missouri. Given its close proximation with the great spring (and fall) flood in Texas, the meteorological context of this event was analyzed through synoptic and ENSO diagnoses for the precipitation event's severity[21]. The synoptic waves that induced the extreme precipitation and ensuing flooding were traced to the Madden Julian Oscillation (MJO), which amplified the trans-Pacific Rossby wave train likely associated with the strong El Niño of December 2015. Though the near historical El Niño contributed to a quasi-stationary trough that induced the high precipitation event, a constructive interference between the MJO and El Niño teleconnections resulted in a relatively weak atmospheric signature of the El Niño. The influence of anthropogenic climate change on the relationship between ENSO and precipitation across central U.S. was revealed from CMIP5 models. Our analysis[21] indicates that a regime change in ENSO-related precipitation anomalies has occurred, from being negatively correlated before 1950 to significantly positive correlations after 1980; this decadal change suggests an effect of anthropogenic warming on the December 2015 deluge in the southern plains. To assess subseasonal predictability, a forecast attribution analysis was conducted using NOAA's Climate Forecast System. Further examination of the MJO's prediction skill shows that the model realistically simulated the spatial patterns and propagation associated with the MJO during December 2015 up to about 20 days in advance with varying prediction skill in different phases of the MJO[21]. This particular study corresponds to the SEED Statement of Need #4 *Using recent historical signals to update the non-stationarity of the climate signal* and it complements the ENSO teleconnection analysis for Texas. It is concluded that the response of precipitation in the southern U.S. to ENSO can be enhanced owing to a warming climate, and we suggested a pathway from which this happens, i.e. the MJO teleconnection compounded by pronounced ENSO phases and its link to the forecast of tropical seasonal variations.

Given the recent extreme flooding in Texas brought about by Hurricane Harvey, we also analyzed this severe precipitation event[17]. Harvey was the first land-falling Category 4 hurricane to hit Texas since Hurricane Carla in September 1961 and it occurred in the absence of any significant ENSO phase. While its intensity at landfall was notable, most of the vast devastation in the Houston metropolitan area was due to Harvey stalling near the southeast Texas coast over several days. As was reported in the project publication[17], Harvey's long-duration rainfall event was reminiscent of extreme flooding that occurred in the neighboring state of Louisiana in 2016: both were caused by a stalled tropical low-pressure system encountering an approaching low-pressure trough from the north. To quantify uncertainty in the attribution of Harvey's rainfall, we used a mesoscale atmospheric model forced by constrained boundary and initial conditions that had their long-term climate trends removed. The removal of the various trends of the boundary and initial conditions minimizes the effects of warming in the air and the ocean surface on Harvey. The 60-member ensemble simulations using a mesoscale model suggest that post-1980 climate warming could have contributed approximately 20% to the extreme precipitation that fell on southeast Texas during 26-29 August 2017, with an interquartile range of 13-37%. This downscaling approach affords the closest means possible of a case-to-case comparison, complementing the more common statistics-based event attribution. Further analysis using the CESM LE to track Harvey-like, stalled tropical low-pressure systems indicates an increase in storm frequency and intensity over southeast Texas through 2050. While the intensification in storm precipitation can be attributed to increased moisture content in the warming troposphere, the increase in storm frequency has some dynamical implication in the changing midlatitude jet stream pattern[22].

c. Characterizing the 4-6-year ENSO propagation processes

We examined the large-scale dynamics of ENSO through the identification and tracking of the so-called conduits or precursor patterns in sea surface temperature (SST) and wind anomaly fields that precede an ENSO event. A chapter of the Ph.D. Dissertation[2] was devoted to explore this aspect. It is known that higher latitudes forcing act through certain conduits or precursor patterns, and they in turn trigger ENSO. These types of precursors have an ocean temperature component either at the surface or subsurface, tapping into the high heat capacity and slow ocean thermal inertia that aids in predictability. The dissertation[2] examined the relationship between two North Pacific ENSO precursor patterns, i.e. the Western North Pacific (WNP) mode and the Pacific Meridional Mode (PMM) and their dynamical evolution, by decomposing (i) the ocean mixed layer heat budget equation and (ii) the vertical mass of the Walker circulation. It is found that, unlike the PMM, the WNP precursor is strongly linked with air-sea heat coupling and ocean advection in the western and equatorial North Pacific; these processes favor the initiation of ocean Kelvin waves favorable for the development of El Niño about a year ahead. In comparison to the PMM, the WNP is more strongly linked to the Pacific Walker circulation, an inherent part of ENSO variability, and tends to last for a longer time than PMM (i.e. making it potentially more predictable).

The processes encompassing the evolution for these two North Pacific ENSO precursors (PMM vs. WNP), as well as their differences, were subsequently studied using the forcing terms of the SST heat budget and diagnostics of the Pacific Walker Circulation variation based on the zonal mass stream function. The result indicates that the WNP (PMM) shows strong air-sea interactions a year (about two season) before the development of a mature ENSO. As shown in Fig. 5, these ENSO precursors are manifest in the advection term of the SST heat budget, which acts in concert with the air-sea heat fluxes to foster ENSO development. These results explain why the peak correlations of wintertime WNP (PMM) with ENSO is maximum at about 4-5 seasons (3 seasons) in advance. The CESM LE analysis replicates a part of the precursors, but more so in the WNP than the PMM (result not shown). However, WNP does exhibit a stronger persistence which translate to potential longer lead time in ENSO prediction. An earlier study[23] has indicated that this WNP connection with ENSO will likely strengthen in the warming climate.

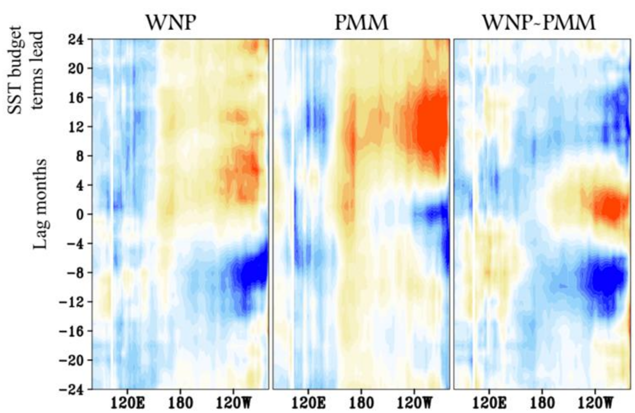

🡐 Fig. 5 Lead/lag regression between ENSO precursor indices (WNP and PMM) and air-sea fluxes (10^{-6} °C s^{-1}) meridionally averaged across 5°S- 5°N with data spanning 1950 to 2015. The strongest anomalies of both the equatorially-averaged air-sea heat fluxes and advection lead the WNP by about 1-2 season. [Adopted from Fosu[2]]

d. Preliminary prediction for Texas' extreme flood risk

Given the outcome of the proposed research[1,3,4], we took the initiative and built a webpage to demonstrate the prediction framework based upon the Indian Ocean→Western Pacific→subtropical North Pacific route of ENSO precursors as proposed[3], as well as the teleconnection from each ENSO phase[4,16]. As shown in Fig. 6 (top), two "decision tree models" were tested using the ERSSTv5 data. "Decision tree" is a decision support tool that uses a tree-like graph or model of decisions and their possible consequences, including the chance of event outcomes. A decision tree model, in the theories of computational complexity and communication complexity, describes the computation or communication process in which an algorithm is developed to sequence the branching of operations based on comparisons of some quantities. Fig. 6 (bottom) shows the webpage hosting the "flood risk" prediction outputted from these decision tree models. There, "High Risk" indicates spring precipitation anomaly in the state of Texas reaching at least 180% above normal, based upon SST anomaly at certain region during certain time. Likewise, Medium Risk (or MidRisk) indicates 90% above normal, while "normal" indicates within 30% of the climatological mean, allowing for a 1-3-year prediction of Texas' spring extreme flood risk. Note that the most current prediction suggests a heightened flood risk in the spring of 2019.

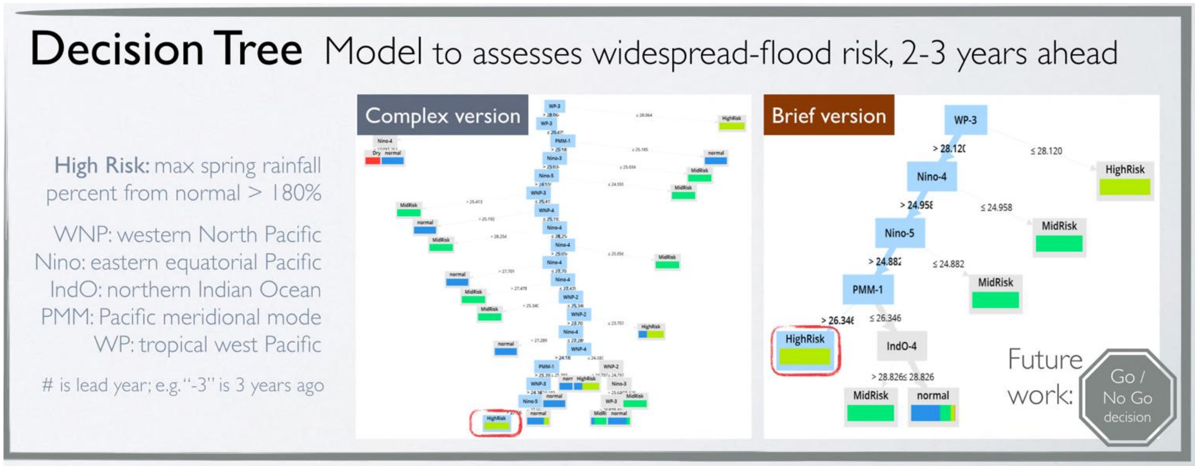

https://earth.climate.usu.edu/service/floodingModel.php (currently under VPN restriction)

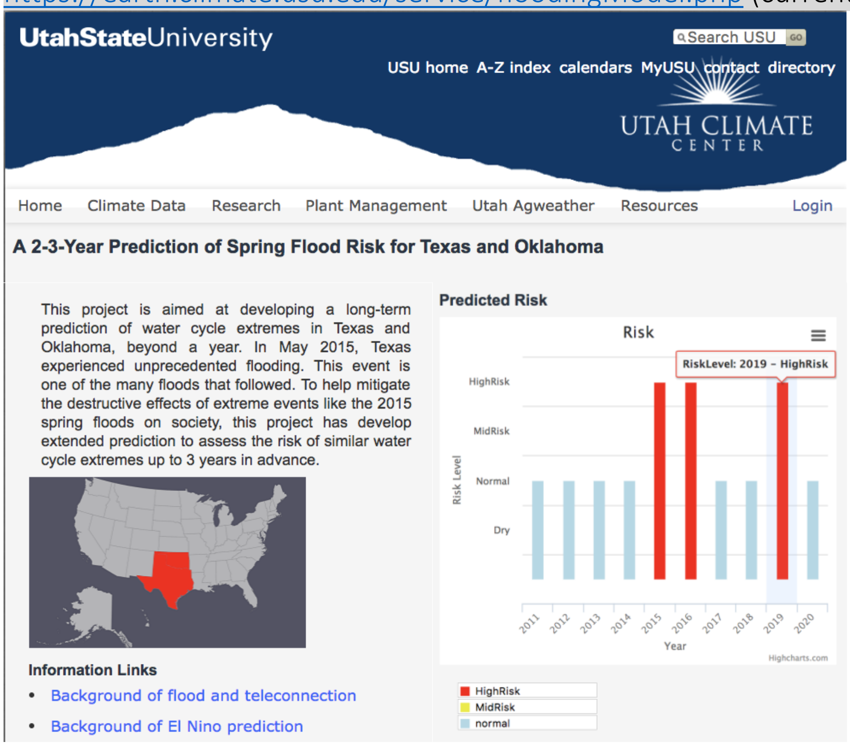

🡐 Fig. 6 (top) The "decision-tree" model concept used to predict extreme flood risks up to 3 years in advance (2018-2020), using SST anomalies of varying seasonal lags according to publications[1,3] that define the SST information. This PI-generated image was presented at the Nov 2017 SERDP Symposium in D.C. (bottom) A preliminary webpage embedded in the Utah Climate Center, illustrating an elevated flood risk for spring 2019 as predicted by the consensus of the above decision-tree models. This website is not yet open for public access.

e. Limitations and caveats to project methodology and results

One has to consider that even a sophisticated model like the CESM remains a limited tool to understand the complicated atmospheric dynamic processes involving interannual variation, global warming and embedded weather extremes. Our initial prediction developed from Wang et al.[3,4] as shown in Fig. 6 is completely empirical (based on decision-tree models with observed information, not yet the dynamic computation). Therefore, improving the prediction still requires independent evaluation of climate model hindcast (forecasts of the past) produced from operational forecast systems to assess dynamical predictability. In terms of the prediction for tropical storms, which is an essential part for the future climate of Texas, we caution that the projection and attribution results found in Wang et al.[17] may differ by model and by the physics schemes used, and its estimate from the downscaling attribution is by no means absolute. Our purpose here is not necessarily to provide a definitive number but rather to propose a way to provide a more quantitative measure of extreme precipitation – i.e. quantifying uncertainty.

5. Conclusions and Implications for Future Research

Objective 1 "*Tracking the 4-6-year ENSO mode and teleconnections*": The present research investigated the large-scale climatic processes (from ocean and the atmosphere) in the occurrence of extreme seasonal precipitation, while examining the compounding factors involving cross-scale interactions in producing Harvey-like extreme flood. Our analysis shown here takes into account that the post-1980 warming is not simply due to anthropogenic causes but also involves natural climate variability *and random weather systems*. Echoing our finding, a recent study[24] based on CO_2 and ENSO as covariates also found that human-induced climate change likely increased Harvey's precipitation in the Houston metropolitan area by 40% with a lower bound estimate of 18%. We note, however, similarly to what they acknowledged in their paper, that other natural modes of variability such as the Atlantic SST anomaly may be responsible for some of the increased SST in the Gulf of Mexico. These are compounding factors that complicate the ENSO-forced variability in Texas and Oklahoma, though our preliminary experiment did indicate potentially skillful prediction of Texas' extreme-flood risk (Fig. 6).

Objective 2 "*Characterizing uncertainty in the 4-6-year prediction*": Our project that analyzed CESM LE and CMIP5 simulations of the future extreme wet and dry seasons and their association with the strengthened ENSO teleconnection under global warming indicate that both intense drought and excessive precipitation will increase towards 2050 with a relatively small inter-model spread. These findings imply that one can take advantage of the recent improvement in ENSO prediction to further the development of long-lead prediction of ENSO's regional climate impact, especially for Texas and vicinity where the signal is robust. Despite the projected increase in annual precipitation, groundwater storage is anticipated to decrease with diminishing groundwater recharge; this is primarily due to the projected increase in summer heat that reduces infiltration. The alternation of wet-dry seasons associated with ENSO can offset the effect of increased precipitation in the long run. Moreover, preliminary CESM analysis projecting stalled storms over Texas, in conjunction with recent analyses of a similarly stalled storm in Louisiana[22], signifies an increasing trend in the number of similar synoptic patterns and stationarity to that accompanying Harvey. This prediction information implies increased duration of heavy rainfall events in the future, despite CESM's relatively coarse resolution that could undermine rainfall intensity.

Implication for future research

Important DoD assets are located in areas where spring rainstorms and hurricanes are evidently becoming more intense, with implication to extreme rainfall and flood risks. Explicitly, the coastal area of Texas where naval bases and airbases are located seems to be one of the most affected facilities in the region. The approach of using process-based prediction for the extreme water cycle coupled with ENSO can graphically express changes in flood risk in a manner that is easily relatable to DoD operational decision-making criteria, such as for issuance of weather watches and warnings. For a better representation of organized convective systems like hurricanes, the US Climate Variability and Predictability Program (CLIVAR) suggests future research to consider utilizing convective permitting modeling that shows superior performance in warm-season convection[25]. We thus call for a careful reevaluation of the projection of both tropical cyclones and spring mesoscale convective systems that may become more frequent, more stalled, and more intense in the future.

In the face of more information coming out of such modeling assessment, it is equally important to examine human cognitive biases in facing climate risk, given the increasing sources of prediction information. Thus, in recommending for a future project, key objectives should include (A) furthering the development of long-lead climate prediction for extreme flood, drought and heat, (B) developing regional prediction products at proper spatial resolution that is useful to military installation sites, and (C) communicating to incentivize management agencies for preparatory actions with emphasis on impacts rather than probability. Potential activity and collaboration of the objectives are identified as follows:

Next-Objective (A): explore the physical processes enabling decadal prediction for extremes

> The task for developing long-lead climate prediction will involve understanding of the interactions between the 4-6-year ENSO cycle and the low-frequency Pacific and Atlantic climate modes, including the less known Pacific Quasi-Decadal Oscillation (QDO)[26,27]. The Pacific QDO's transition phase between extreme warm and cold in SSTA can induce impactful teleconnection patterns that significantly modulate the U.S. hydroclimate[28], as we had reported on the Great Missouri River flood[29]. As recent as 2018, a similar approach based on low-frequency climate variability concerning ENSO has been applied to accessing Mississippi River's river engineering and how it impacts flood hazard[30]. This task will be conducted primarily by the PI's group at Utah State University.

Next-Objective (B): analyze past/future conditions at high resolution for specific sites

> Any useful prediction information of climate needs to be interpreted to proper geographical boundary that is meaningful to installation management. To produce physically sound interpretation of climate risks (dynamic downscaling), high-resolution computer modeling is necessary in order to quantify any risk level at certain locations. This task will be joined by the 2017 SERDP Project of The Year (RC-2205) team led by Dr. Christopher L. Castro of University of Arizona, to produce dynamically downscaled prediction for the risk of extreme events. The PI has collaborated with Dr. Castro in the past three years and together they serve in the U.S. CLIVAR's Predictability, Predictions,

and Applications Interface Panel (https://usclivar.org/panels/ppai), a national research program that fosters understanding and prediction of climate variability. By teaming up, Dr. Castro and the PI will investigate how the predicted change in the atmospheric environment of next 2-5 years affect Texas' rainy season (pattern change and storm behavior) extracted from global climate models using convective-permitting models.

Next-Objective (C): communicate to develop information requirements by discipline and location

This task is focused on avoiding the recently found five "decision biases"[31] that interfere with management's ability to minimize installation damage: (1) spatial myopia, (2) poor mental model of risk, (3) gaps between objective and subjective probability estimates, (4) prior event experience, and (5) political factors. These biases can only be reduced through effective communication linking a predicted risk with the perceived risk. The PI will work with a journalism professor, Dr. Matthew D. LaPlante (hyperlink) of Utah State University, who is ex-Navy and has done combat correspondence and veterans affairs reporting. Specialized in "crisis communication", Dr. LaPlante will analyze the prediction information versus historic/perceived events and then, tailor the prediction information into consequential impacts for practitioners to weight in; this will help mitigate cognitive biases that come into play on long and short time scales when managers make preparation decisions[31]. We will offer a framework for improved decision making in the face of the above five biases to reduce vulnerability to extreme events. Dr. LaPlante is best for this task for his professional work experience in international crises, military issues, and science, reported from a dozen nations including Iraq.

Affirmation of final report

The information presented in this interim technical report represents an accurate reporting of the most pertinent research results obtained in Project RC-2709 (Limited Scope) in relation to the originally proposed work, to the conclusion of funding period of this project.

Simon S.-Y. Wang, Ph.D.

Principal Investigator

Literature Cited:

1 Yoon, J.-H., S.-Y. Wang, M.-H. Lo, and W.-Y. Wu. Concurrent increases in wet and dry extremes projected in Texas and combined effects on groundwater. *Environmental Research Letters*, DOI: 10.1088/1748-9326/aab1096b (2018).

2 Fosu, B. *Towards the Prediction of Climate Extremes with Attribution Analysis Through Climate Diagnostics and Modeling: Cases from Asia to North America* PhD thesis, Utah State University, (2018).

3 Wang, S.-Y., Jiang, X. & Fosu, B. Global eastward propagation signals associated with the 4–5-year ENSO cycle. *Climate Dynamics* **44**, 2825-2837 (2015).

4 Wang, S.-Y., Huang, W.-R., Hsu, H.-H. & Gillies, R. R. Role of the strengthened El Niño teleconnection in the May 2015 floods over the southern Great Plains. *Geophysical Research Letters* **42**, 8140-8146, doi:10.1002/2015GL065211 (2015).

5 Wang, S.-Y., L'Heureux, M. & Chia, H.-H. ENSO prediction one year in advance using western North Pacific sea surface temperatures. *Geophys. Res. Lett.* **39**, L05702, doi:10.1029/2012gl050909 (2012).

6 Capotondi, A. & Sardeshmukh, P. D. Optimal precursors of different types of ENSO events. *Geophysical Research Letters* **42**, 9952-9960 (2015).

7 Meehl, G. A. & Teng, H. Multi-model changes in El Niño teleconnections over North America in a future warmer climate. *Climate dynamics* **29**, 779-790 (2007).

8 Stevenson, S. *et al.* Will there be a significant change to El Niño in the twenty-first century? *Journal of Climate* **25**, 2129-2145 (2012).

9 van Oldenborgh, G. J. *et al.* Attribution of extreme rainfall from Hurricane Harvey, August 2017. *Environmental Research Letters* **12**, 124009 (2017).

10 Fernando, D. N. *et al.* What caused the spring intensification and winter demise of the 2011 drought over Texas? *Climate dynamics* **47**, 3077-3090 (2016).

11 Nielsen-Gammon, J. W. The 2011 Texas drought. *Texas Water Journal* **3**, 59-95 (2012).

12 Rupp, D. *et al.* Did human influence on climate make the 2011 Texas drought more probable. *Bulletin of the American Meteorological Society* **93**, 1052-1054 (2012).

13 Yu, J.-Y., Sun, F. & Kao, H.-Y. Contributions of Indian Ocean and monsoon biases to the excessive biennial ENSO in CCSM3. *Journal of Climate* **22**, 1850-1858 (2009).

14 Bellenger, H., Guilyardi, E., Leloup, J., Lengaigne, M. & Vialard, J. ENSO representation in climate models: from CMIP3 to CMIP5. *Climate Dynamics* **42**, 1999-2018 (2014).

15 Kay, J. *et al.* The Community Earth System Model (CESM) large ensemble project: A community resource for studying climate change in the presence of internal climate variability. *Bulletin of the American Meteorological Society* **96**, 1333-1349 (2015).

16 Yoon, J.-H. *et al.* Increasing water cycle extremes in California and in relation to ENSO cycle under global warming. *Nature communications* **6**, DOI: 10.1038/ncomms9657 (2015).

17 S.-Y. Wang, L. Z., Jin-Ho Yoon, Phil Klotzbach, and Robert R. Gillies. Attribution of climate effects on Hurricane Harvey's extreme rainfall in Texas. *Environmental Research Letters*, DOI:10.1088/1748-9326/aabb1085 (2018).

18 Kalnay, E. *et al.* The NCEP/NCAR 40-Year Reanalysis Project. *Bulletin of the American Meteorological Society* **77**, 437-471, doi:doi:10.1175/1520-0477(1996)077<0437:TNYRP>2.0.CO;2 (1996).

19 Smith, T. M. & Reynolds, R. W. Extended Reconstruction of Global Sea Surface Temperatures Based on COADS Data (1854-1997). *Journal of Climate* **16**, 1495-1510, doi:10.1175/1520-0442-16.10.1495 (2003).

20 Chen, M., Xie, P., Janowiak, J. E. & Arkin, P. A. Global Land Precipitation: A 50-yr Monthly Analysis Based on Gauge Observations. *Journal of Hydrometeorology* **3**, 249-266, doi:10.1175/1525-7541(2002)003<0249:glpaym>2.0.co;2 (2002).

21 Fosu, B., Wang, S. & Pegion, K. Synoptic and Climate Attributions of the December 2015 Extreme Flooding in Missouri, USA. *Water* **10**, 350 (2018).
22 Wang, S.-Y., Zhao, L. & Gillies, R. R. Synoptic and quantitative attributions of the extreme precipitation leading to the August 2016 Louisiana flood. *Geophysical Research Letters* **43**, 11,805-811,814, doi:10.1002/2016GL071460 (2016).
23 Wang, S.-Y., L'Heureux, M. & Yoon, J.-H. Are Greenhouse Gases Changing ENSO Precursors in the Western North Pacific? *Journal of Climate* **26**, 6309-6322, doi:10.1175/JCLI-D-12-00360.1 (2013).
24 Risser, M. D. & Wehner, M. F. Attributable Human-Induced Changes in the Likelihood and Magnitude of the Observed Extreme Precipitation during Hurricane Harvey. *Geophysical Research Letters* **44**, 12,457-412,464, doi:10.1002/2017GL075888 (2017).
25 US_CLIVAR. 2017 US CLIVAR Summit Report. 38, doi:10.5065/D5066CJ5068C5064 (US CLIVAR Project Office, 2017).
26 Wang, S.-Y., Gillies, R. R., Hipps, L. E. & Jin, J. A transition-phase teleconnection of the Pacific quasi-decadal oscillation. *Clim. Dynamics* **36**, 681-693, doi:10.1007/s00382-009-0722-5 (2011).
27 White, W. B. & Cayan, D. R. A global El Niño-Southern Oscillation wave in surface temperature and pressure and its interdecadal modulation from 1900 to 1997. *Journal of Geophysical Research: Oceans (1978–2012)* **105**, 11223-11242 (2000).
28 Wang, S.-Y., Gillies, R. R. & Reichler, T. Multi-decadal drought cycles in the Great Basin recorded by the Great Salt Lake: Modulation from a transition-phase teleconnection. *Journal of Climate* **25**, 1711-1721, doi:10.1175/2011jcli4225.1 (2012).
29 Wang, S.-Y., Hakala, K., Gillies, R. R. & Capehart, W. J. The Pacific quasi-decadal oscillation (QDO): An important precursor toward anticipating major flood events in the Missouri River Basin? *Geophysical Research Letters* **41**, 2013GL059042, doi:10.1002/2013GL059042 (2014).
30 Munoz, S. E. *et al.* Climatic control of Mississippi River flood hazard amplified by river engineering. *Nature* **556**, 95, doi:10.1038/nature26145 (2018).
31 Milch, K., Broad, K., Orlove, B. & Meyer, R. Decision Science Perspectives on Hurricane Vulnerability: Evidence from the 2010–2012 Atlantic Hurricane Seasons. *Atmosphere* **9**, 32 (2018).

IOP Publishing Environ. Res. Lett. 13 (2017) 054002 https://doi.org/10.1088/1748-9326/aab96b

Environmental Research Letters

CrossMark

OPEN ACCESS

RECEIVED
1 December 2017

REVISED
19 March 2018

ACCEPTED FOR PUBLICATION
26 March 2018

PUBLISHED
20 April 2018

LETTER

Concurrent increases in wet and dry extremes projected in Texas and combined effects on groundwater

Jin-Ho Yoon[1,6], S-Y Simon Wang[2,3], Min-Hui Lo[4] and Wen-Ying Wu[5]

1 School of Earth Sciences and Environmental Engineering, Gwangju Institute of Science and Technology, Gwangju, South Korea
2 Department of Plants, Soils, and Climate, Utah State University, Logan, UT, United States of America
3 Utah Climate Center, Utah State University, Logan, UT, United States of America
4 Department of Atmospheric Sciences, National Taiwan University, Taipei, Taiwan
5 Department of Geological Sciences, Jackson School of Geosciences, The University of Texas at Austin, TX, United States of America
6 Author to whom any correspondence should be addressed.

E-mail: yjinho@gist.ac.kr

Keywords: climate extremes, ENSO, drought, flood

Supplementary material for this article is available online

Abstract

The US state of Texas has experienced consecutive flooding events since spring 2015 with devastating consequences, yet these happened only a few years after the record drought of 2011. Identifying the effect of climate variability on regional water cycle extremes, such as the predicted occurrence of La Niña in winter 2017–2018 and its association with drought in Texas, remains a challenge. The present analyses use large-ensemble simulations to project the future of water cycle extremes in Texas and assess their connection with the changing El Niño–Southern Oscillation (ENSO) teleconnection under global warming. Large-ensemble simulations indicate that both intense drought and excessive precipitation are projected to increase towards the middle of the 21st century, associated with a strengthened effect from ENSO. Despite the precipitation increase projected for the southern Great Plains, groundwater storage is likely to decrease in the long run with diminishing groundwater recharge; this is due to the concurrent increases and strengthening in drought offsetting the effect of added rains. This projection provides implications to short-term climate anomaly in the face of the La Niña and to long-term water resources planning.

1. Introduction

Before Hurricane Harvey hit the US state of Texas in August 2017, heavy precipitation events of non-hurricane origins have already caused multiple floods since April 2015 with devastating consequences. The May 2015 flood resulted from over 400 mm above-normal rainfall falling on Texas (Wang *et al* 2015). Then, the May 2016 flood took 12 lives and caused historic river levels, making it the fifth major flood event and the second 500 year flood in the Houston area. As shown in figure 1(*a*), the precipitation anomaly over the 13 months from May 2015 through May 2016 reveals a marked increase centered around Oklahoma, which is the upstream of many rivers that run through the southern Great Plains (SGP). The timing of these recent spring floods coincides with SGP's rainy season (figure 1(*b*)). Starting in April, a 'spring trough' develops west of the SGP and it interacts with the developing low-level jet (LLJ) to form the convergence of moisture fluxes (Helfand and Schubert 1995), leading to the May–June rainfall peak over the SGP (Higgins *et al* 1997, Wang and Chen 2009). The synoptic conditions associated with floods in 2015 and 2016 during April–June (AMJ, defined for spring) are not too distinct from each other, both featuring a quasi-stationary trough west of the SGP (supplemental figure S1 available at stacks.iop.org/ERL/13/054002/mmedia) generating short waves and squall lines. In May 2015, the developing El Niño further deepened this quasi-stationary trough while enhancing the LLJ (Wang *et al* 2015). Global warming acted to strengthen the El Niño teleconnection (Meehl and Teng 2007, Stevenson *et al* 2012) that affects the SGP. Hurricanes such as Harvey also produce excessive rainfall and can lead to flood, but these weather systems are random

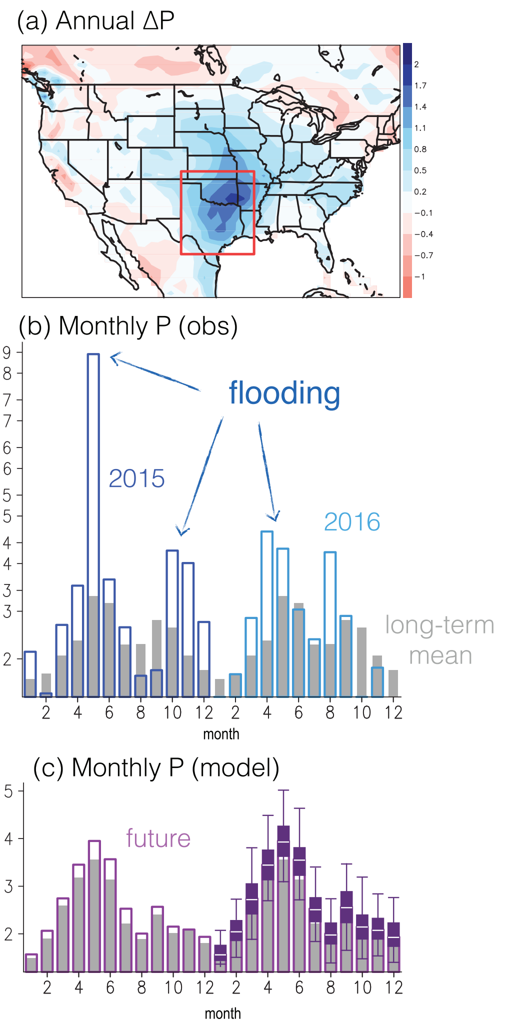

Figure 1. (*a*) Annual mean precipitation anomalies of May 2015 through May 2016 from the climatology (mm/day). (*b*) Monthly precipitation averaged in the SGP as outlined in (*a*) for the climatology (gray bar) and the 2015–2016 period (open blue bar), repeated for one more annual cycle for illustration. (*c*) Similar to (*b*) but for the CESM LE precipitation of the historical period (gray bar) and future period (open bar); the ensemble spread is overlaid with the second annual cycle as the box plot.

in nature and linking them to large-scale forcing is difficult (van Oldenborgh *et al* 2017).

The succession of the post-2014 floods in Texas could lead the society into overlooking the risk in the comeback of severe droughts. In 2011, Texas underwent an intense drought and associated heat waves that was unprecedented (Nielsen-Gammon 2012) making it the worst 1 year drought on record (Fernando *et al* 2016). Both the strong La Niña and anthropogenic warming played a role in the severity and increased probability of this record drought (Rupp *et al* 2012), suggesting that the El Niño-related 2015 flood is the opposite pattern of the 2011 drought. Given the robust influence of the El Niño–Southern Oscillation (ENSO) on the SGP's precipitation (Lee *et al* 2014, Liang *et al* 2014, Liang *et al* 2015) and the role of global warming in strengthening this ENSO influence (Rupp *et al* 2012, Stevenson *et al* 2012, Wang *et al* 2015), it is reasonable to anticipate a drying tendency, or even drought, to occur over the SGP in the face of a (future) La Niña event.

As of November 2017, the NOAA Climate Prediction Center (CPC) indicated a 70% chance for a La Niña to develop through February 2018. Given the emergence of this La Niña event, we decided to analyze the risk of severe drought to occur in the SGP, similar to that of the 2011 condition, and evaluate climate model projections of its water cycle extremes represented by excessive wet season and severe drought.

2. Data sources

Forty members of climate simulation were produced by the Community Earth System Model version 1's Large Ensemble Project (CESM-LE) with spatial resolution of 0.9 degrees longitude x 1.25 degrees latitude (Kay *et al* 2015). The simulations cover two periods: (1) 1920–2005 with historical forcing including greenhouse gases, aerosol, ozone, land use change, solar and volcanic activity, and (2) 2006–2080 with RCP8.5 forcing (Taylor *et al* 2012). The ensemble spread of initial conditions is generated by the commonly used 'round-off differences' method (Kay *et al* 2015). CESM-LE was used here partly because it performs well on the depiction of the ENSO cycle and its teleconnection over the North Pacific and North America (Wang *et al* 2015, Yoon *et al* 2015). Of note, the land surface model used in the CESM-LE does not include the process of anthropogenic groundwater withdrawal.

For observational data, we use the NCEP/NCAR Reanalysis (R1) (Kalnay *et al* 1996) that starts in 1948 in order to analyze interdecadal changes. Other datasets include the Extended Reconstructed Sea Surface Temperature (ERSST, v3b) derived from the International Comprehensive Ocean–Atmosphere Dataset (Smith and Reynolds 2003) for the ENSO indexing and the NOAA Precipitation Reconstruction over Land (PREC/L) gridded product (Chen *et al* 2002) of 0.5° degree resolution.

3. Results

Based on the SGP domain outlined in figure 1(*a*), the CESM-LE simulation of the region's monthly precipitation is shown in figure 1(*c*) for the historical (1940–1985) and a 'near-future' (2010–2060) periods. In terms of climatology, CESM-LE captured the spring rainy season but underestimates the secondary rainfall peak in fall. Overall, precipitation in the SGP is projected to increase throughout the year with a larger increase in spring (April–June or AMJ), in which the precipitation increase amounts to 15%–20%. Subsequently, we examine the El Niño impact on the SGP's spring precipitation based upon the precipitation composites; this is determined by the sea surface temperature anomalies (SSTA) of the NINO3.4

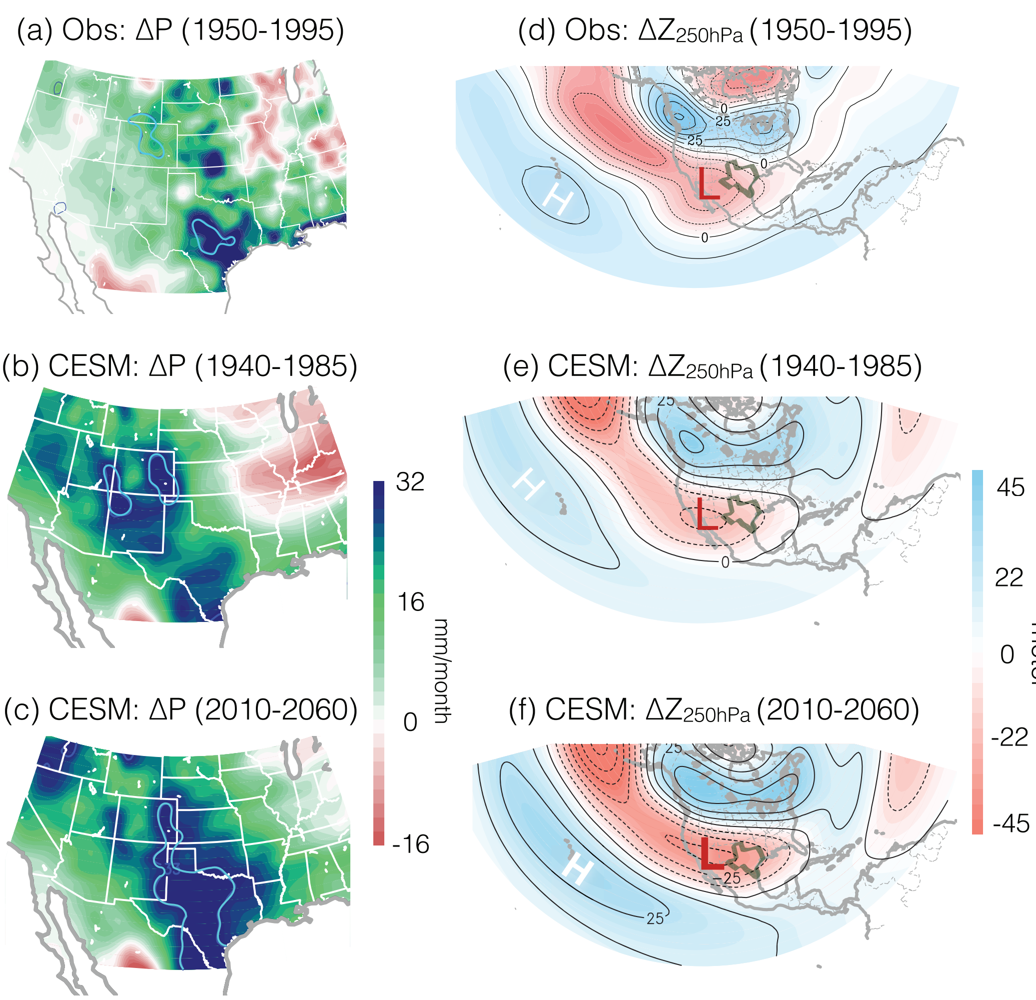

Figure 2. Ensemble precipitation differences (P) between the El Niño and La Niña composites (see text) during the April–June seasons of (*a*) 1940–1985 and (*b*) 2010–2060; the blue contours outline the significance level of $p < .001$. (*c*)–(*d*) Similar to (*a*)–(*b*) but for the 250 hPa geopotential height difference (ΔZ) ensembles for the same two periods.

region (170°–140°W, 5°S–5°N) being greater than 0.5 °C in the spring and 1 °C in the preceding winter (less than −0.5 °C/-1 °C for La Niña). This threshold is applied to each ensemble member and the observation as well, to depict the difference of the precipitation composites between El Niño and La Niña. The observational analysis during 1950–1995 (figure 2(*a*)) shows anomalous precipitation over southeastern Texas and part of Oklahoma and Louisiana, a known feature. In the near-future simulations (figure 2(*c*)) and the historical simulations (figure 2(*b*)), there is a marked increase in the ensemble mean precipitation composite difference between El Niño and La Niña in the SGP. Furthermore, a similar precipitation analysis using the Coupled Model Intercomparison Project Phase 5 (CMIP5), which is shown in supplemental figure S2 by following Wang *et al* (2015), reveals corresponding precipitation patterns as well. That both the CESM-LE and CMIP5 simulations capture the general pattern and intensification of the ENSO-related precipitation anomalies in the SGP suggests an impact from anthropogenic climate warming.

In terms of the atmospheric circulation associated with ENSO and its changing teleconnection, figures 2(*e*) and (*f*) show the CESM-LE-generated geopotential height differences at 250 hPa; these are generally in agreement with the observed pattern in figure 2(*d*) including the synoptic trough west of Texas. The El Niño-associated low-pressure anomaly west of Texas is enhanced by about 35% during 2010–2060 (figure 2(*f*)), while the broad-scale teleconnection pattern remains similar to the historical simulations (figure 2(*e*)). We should note that a sign reversal in figure 2 indicates the La Niña influence on precipitation reduction in Texas. We should note that seasonal rainfall anomalies in the SGP are not only controlled by ENSO but by other circulation factors as well. Nonetheless, a further sliding correlation analysis between the SGP precipitation and the ENSO cycle, based on different climate models and a different precipitation observation, yields the same outcome of an amplified ENSO impact (supplemental figure S2).

Next, we examine the prevailing circulation pattern modulating the SGP by plotting in figure 3 the anomalous 250 h Pa geopotential height that is regressed

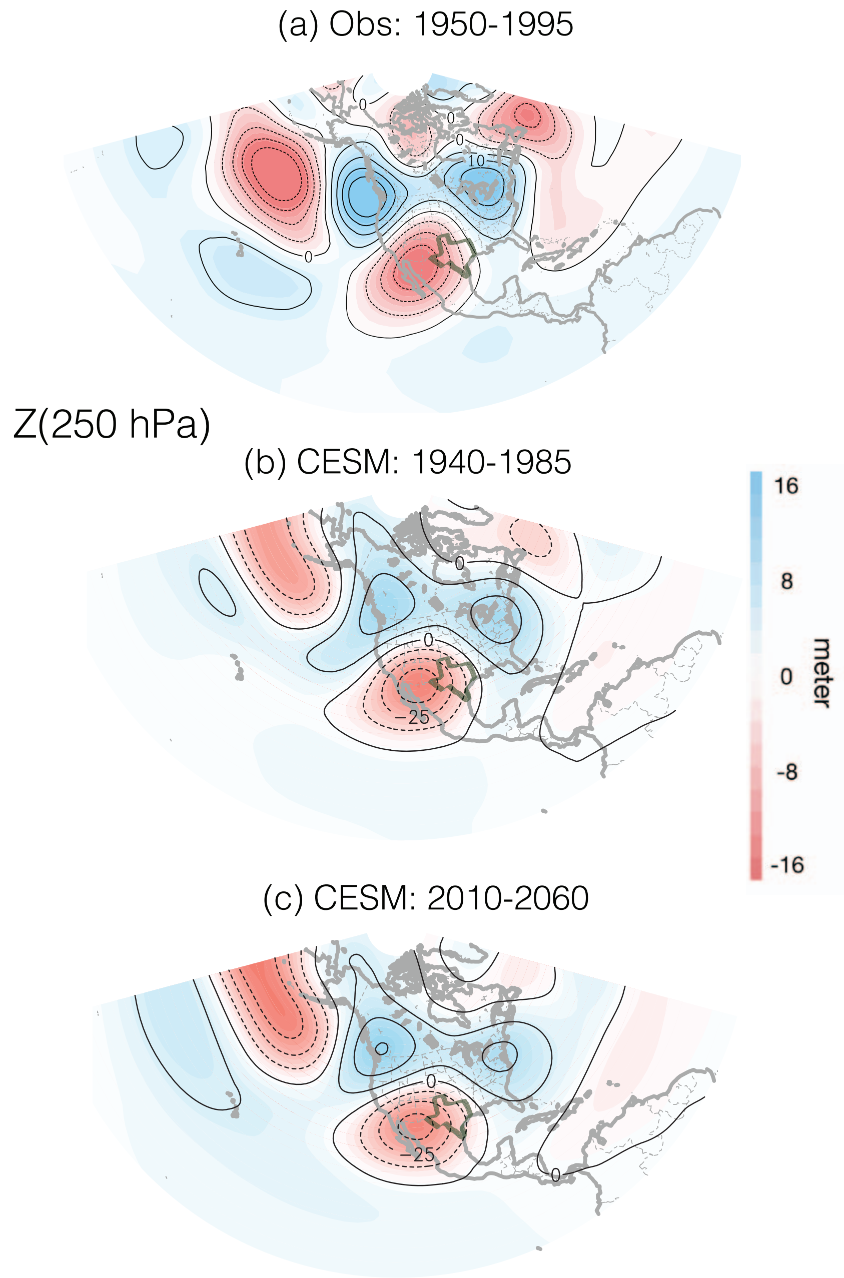

Figure 3. CESM LE's 250 hPa geopotential height anomalies (ΔZ) regressed with the normalized spring precipitation averaged in Texas (outlined) for the periods of (*a*) 1940–1985 and (*b*) 2010–2060 during the April–June season.

with the SGP precipitation during AMJ. A low-pressure anomaly to the west of Texas appears to be the dominant feature embedded in a zonally oriented short-wave train, which is different from the long-wave dominant pattern induced by ENSO (figures 2(*d*)–(*f*)). There is not an apparent difference in the anomalous circulation's magnitude over Texas between the two time periods, suggesting that the common circulation features affecting the spring precipitation in Texas will not change. However, the strengthened ENSO teleconnection can become increasingly important to modulate or amplify this circulation feature. We should also note that other major circulation processes may compensate the ENSO teleconnection and that the sample sizes between figures 2 and 3 are different.

To examine the changing association between spring precipitation anomalies in the SGP and the ENSO cycle, we next compute the precipitation's 15 year sliding correlations with the spring NINO3.4 SSTA from the observation and CESM-LE data; this is shown in figure 4(*a*). There is a clear decadal-scale fluctuation in the observation with a more pronounced increase after year 2000. The CESM-LE produces a gradual increase and it becomes persistently significant after 2000, at the 95% level. These results echo Wang *et al* (2015)'s observational and modeling analyses that the SGP's spring precipitation response to the ENSO teleconnection has intensified and this trend is projected to continue. Other recent studies (Guilyardi *et al* 2012, Yoon *et al* 2015,

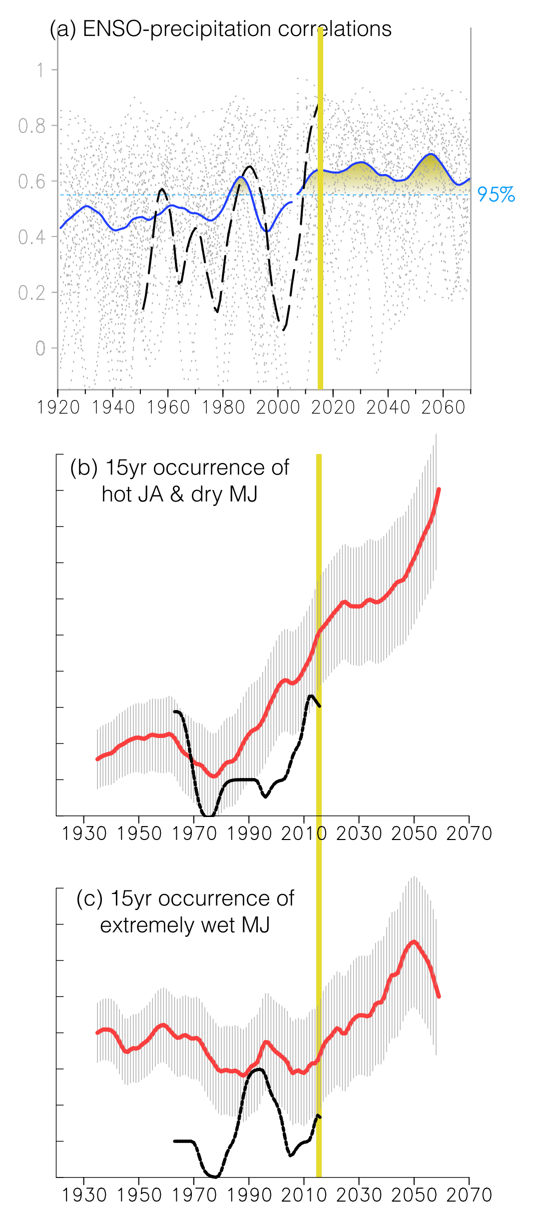

Figure 4. (*a*) The 15 year sliding correlations between the spring precipitation in the SGP and the NINO3.4 SSTA derived from both the observation (black broken line) and CESM LE (blue line), overlaid with individual members as light gray dashed lines. The values above the 95% significance interval is shaded with yellow. (*b*) The 15 year concurrences of a hot summer following a dry spring computed from the observation (black line) and CESM LE (red line) and the ensemble spread (error bar). (*c*) Same as (*b*) but for the 15 year running occurrence of extremely wet springs in the SGP.

Zhou *et al* 2014) also suggest that the changing tropical heat release associated with the ENSO-related teleconnection has amplified its regional impacts worldwide.

Perhaps a greater implication of these analyses can be revealed by the concurrence of a hot summer following a dry spring, loosely describing a flash drought in the central US (Otkin *et al* 2016). Here, hot summers are defined as the July–September (JAS) surface air temperature exceeding 1 standard deviation (sd.) above the mean, while dry springs refer the AMJ precipitation deficit of 1 sd. below the mean of either era; these are computed within a 15 year running window. This analysis is based on the fact that severe drought in the SGP usually accompanies a below-normal spring/rainy season followed by a hotter-than-normal summer season (Long *et al* 2013, Nielsen-Gammon 2012). As shown in figure 4(*b*), the observed drought occurrence has increased after the 1990s, though it appears to be part of a multi-decadal variation. In the CESM-LE, the drought occurrence increases persistently throughout the 21st century. Likewise, the 15 year running occurrence of extremely wet springs (figure 4(*c*); defined by the AMJ precipitation deficit of 2 sd. below the mean), is projected to increase after 2015 despite a downtrend after 2050. By comparing figures 4(*b*) with (*c*), it appears that the disparity between their latter trends is caused by a further increase in dry springs. This downtrend in figure 4(*c*) is likely due to internal model variability such as that drives the earlier turnarounds in the historical period. Regardless, the ENSO impact on the JAS precipitation change in the SGP is also projected to amplify, as shown in supplemental figure S3 following the composites of figures 2(*c*) and (*d*).

To quantify the effect of the changing ENSO teleconnection on the extreme wet/dry spring and summer in the SGP, we further compute the frequencies of (a) back-to-back wet springs consisting of AMJ precipitation anomalies greater than 1 sd. occurring in two consecutive years, (b) same as (a) but only for those occurring with an El Niño winter in between, and (c) reversal of (b) for consecutive two dry summers with the JAS precipitation deficits below 1 sd. occurring with a La Niña winter in between; these are computed within a 30 year window and shown in figure 5. In the observation, the period of 1985–2015 exhibits a distinctly higher frequency in all three cases than the earlier 30 years. Meanwhile, the CESM-LE projects an almost linear increase in both the El Niño-associated wet springs and the La Niña-accompanied dry summers toward the end of the 21st century. Given the difference between the observation and CESM-LE simulations revealed in figures 4 and 5, one has to take into account that even a sophisticated model like the CESM-LE remains a limited tool to understand the complicated climatological processes involving interannual variation, global warming and associated extremes.

4. Implication on groundwater

At face value, an increasingly wet climate in the SGP (cf. figure 1(*c*)) would suggest a net increase in the water storage, but how the concurrent increase in dry summers affect the groundwater storage in the SGP in the future remains unclear. Analyzing the CESM-LE's groundwater outputs, the trends of the 1956–2080 period are computed for groundwater storage anomalies and groundwater recharge. The

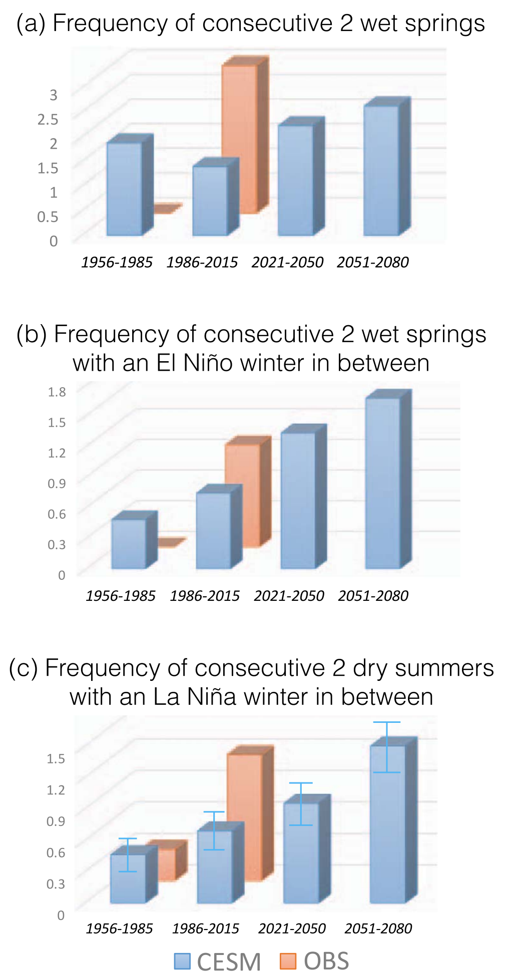

Figure 5. The 30 year frequencies of (*a*) consecutive two wet springs, (*b*) same as (*a*) but with an El Niño winter in between, and (*c*) consecutive two dry summers with a La Niña winter in between, computed from the observation (orange) and CESM LE data (blue).

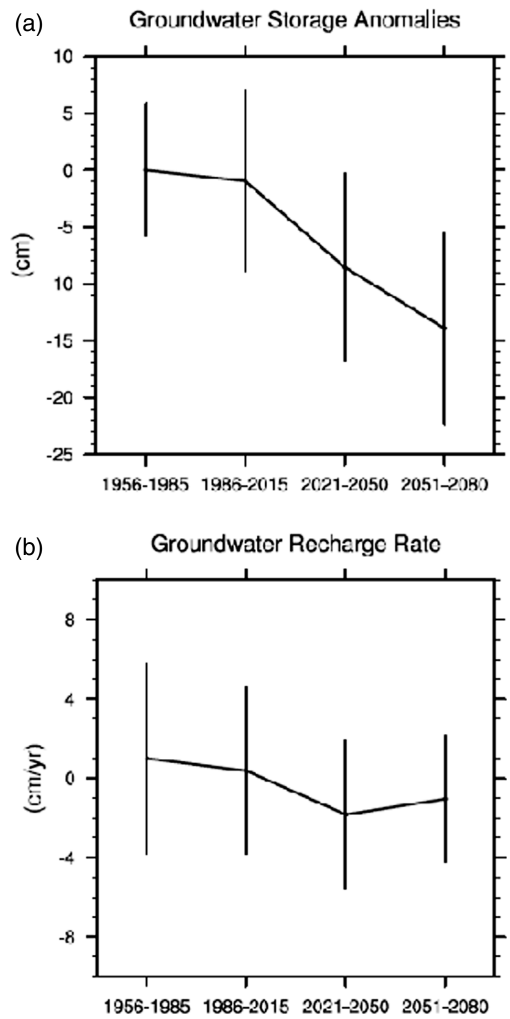

Figure 6. (*a*) CESM LE's groundwater storage anomalies over the SGP relative to 2006 values in the ensemble mean (line) and model spread (shading). (*b*) The 30 year means of the CESM LE groundwater recharge rate with the model spread in error bars.

simulated groundwater storage anomalies are shown in figure 6(*a*) from 1956–2080 averaged every 30 year, relative to the mean of 1956–1985. The result indicates a significant decrease with a rate of approximately −1.5 cm per decade in the future. Figure 6(*b*) shows the simulated groundwater recharge rate from 1956–2080, in which the decline in the recharge rate becomes negative after around 2015. While an increase in annual precipitation is projected in the SGP, it seems that the increase in surface evapotranspiration plays a substantial role in affecting the terrestrial water budget; this leads to a smaller infiltration and a reduction in the groundwater recharge and soil water.

5. Concluding remarks

The US southern Great Plains has experienced an alternation of severe drought and extreme flood since 2010 with devastating consequences. We have analyzed large-ensemble simulations that project the future of extreme wet and dry seasons in the SGP and assessed their association with the changing ENSO teleconnection under global warming. Both intense drought and excessive precipitation are projected to increase towards the middle of the 21st century and this projection is associated with a strengthened relation with ENSO teleconnections. The findings presented here echo the documented effect of El Niño in strengthening the anthropogenic warming-induced increase in summer rainfall elsewhere in the world, such as central China (Yuan *et al* 2018). Despite the projected increase in precipitation over the SGP, groundwater storage is anticipated to decrease with diminishing groundwater recharge; this is primarily due to the surface warming and projected increase in summer drought that reduces infiltration. These, subsequently, offset the effect of increased precipitation. The analysis presented here may be model-dependent and requires further verification using more sophisticated land surface models and/or subsurface observations.

Acknowledgments

J Yoon was supported by the funding from the Korean Meteorological Administration Research and Development Program under Grant KMI2017–2410. SY Wang was supported by the SERDP grant RC-2709. M Lo acknowledged funding MOST 106-2111-M-002-010-MY4.

ORCID iDs

Jin-Ho Yoon https://orcid.org/0000-0002-4939-8078

References

Chen M, Xie P, Janowiak J E and Arkin P A 2002 Global land precipitation: a 50 yr monthly analysis based on gauge observations *J. Hydrometeorol.* **3** 249–66

Fernando D N, Mo K C, Fu R, Pu B, Bowerman A, Scanlon B R, Solis R S, Yin L, Mace R E and Mioduszewski J R 2016 What caused the spring intensification and winter demise of the 2011 drought over Texas? *Clim. Dyn.* **47** 3077–90

Guilyardi E, Bellenger H, Collins M, Ferrett S, Cai W and Wittenberg A 2012 A first look at ENSO in CMIP5 *Clivar Exchanges* **17** 29–32

Helfand H M and Schubert S D 1995 Climatology of the simulated great plains low-level jet and its contribution to the continental moisture budget of the United States *J. Clim.* **8** 784–806

Higgins R, Yao Y, Yarosh E, Janowiak J E and Mo K 1997 Influence of the great plains low-level jet on summertime precipitation and moisture transport over the central United States *J. Clim.* **10** 481–507

Kalnay E *et al* 1996 The NCEP/NCAR 40 year reanalysis project *Bull. Am. Meteorol. Soc.* **77** 437–71

Kay J, Deser C, Phillips A, Mai A, Hannay C, Strand G, Arblaster J, Bates S, Danabasoglu G and Edwards J 2015 The community earth system model (CESM) large ensemble project: a community resource for studying climate change in the presence of internal climate variability *Bull. Am. Meteorol. Soc.* **96** 1333–49

Lee S-K, Mapes B E, Wang C, Enfield D B and Weaver S J 2014 Springtime ENSO phase evolution and its relation to rainfall in the continental US *Geophys. Res. Lett.* **41** 2013GL059137

Liang Y-C, Lo M-H and Yu J-Y 2014 Asymmetric responses of land hydroclimatology to two types of El Niño in the Mississippi River Basin *Geophys. Res. Lett.* **41** 582–8

Liang Y-C, Yu J-Y, Lo M-H and Wang C 2015 The changing influence of El Niño on the great plains low-level jet *Atmos. Sci. Lett.* **16** 512–17

Long D, Scanlon B R, Longuevergne L, Sun A Y, Fernando D N and Save H 2013 GRACE satellite monitoring of large depletion in water storage in response to the 2011 drought in Texas *Geophys. Res. Lett.* **40** 3395–401

Meehl G A and Teng H 2007 Multi-model changes in El Niño teleconnections over North America in a future warmer climate *Clim. Dyn.* **29** 779–90

Nielsen-Gammon J W 2012 The 2011 Texas drought *Texas Water J.* **3** 59–95

Otkin J A, Anderson M C, Hain C, Svoboda M, Johnson D, Mueller R, Tadesse T, Wardlow B and Brown J 2016 Assessing the evolution of soil moisture and vegetation conditions during the 2012 United States flash drought *Agric. Forest Meteorol.* **218** 230–42

Rupp D, Mote P, Massey N, Rye C, Jones R and Allen M 2012 Did human influence on climate make the 2011 Texas drought more probable *Bull. Am. Meteorol. Soc.* **93** 1052–4

Smith T M and Reynolds R W 2003 Extended reconstruction of global sea surface temperatures based on COADS data (1854–1997) *J. Clim.* **16** 1495–510

Stevenson S, Fox-Kemper B, Jochum M, Neale R, Deser C and Meehl G 2012 Will there be a significant change to El Niño in the twenty-first century? *J. Clim.* **25** 2129–45

Taylor K E, Stouffer R J and Meehl G A 2012 An overview of CMIP5 and the experiment design *Bull. Am. Meteorol. Soc.* **93** 485–98

van Oldenborgh G J, van der Wiel K, Antonia S, Roop S, Julie A, Friederike O, Karsten H, Sihan L, Gabriel V and Heidi C 2017 Attribution of extreme rainfall from Hurricane Harvey, August 2017 *Environ. Res. Lett.* **12** 124009

Wang S-Y and Chen T-C 2009 The late-spring maximum of rainfall over the US central plains and the role of the low-level jet *J. Clim.* **22** 4696–709

Wang S-Y, Huang W-R, Hsu H-H and Gillies R R 2015 Role of the strengthened El Niño teleconnection in the May 2015 floods over the southern Great Plains *Geophys. Res. Lett.* **42** 8140–6

Yoon J-H, *et al* 2015 Increasing water cycle extremes in California and relation to ENSO cycle under global warming *Nat. Commun.* **6** 8657

Yuan X, Wang S and Hu Z-Z 2018 Do climate change and El Niño increase likelihood of Yangtze River extreme rainfall? *Bull. Am. Meteorol. Soc.* S113–7

Zhou Z-Q, Xie S-P, Zheng X-T, Liu Q and Wang H 2014 Global warming–induced changes in El Niño teleconnections over the North Pacific and North America *J. Clim.* **27** 9050–64

Appendix - project paper #2

IOP Publishing Environ. Res. Lett. 13 (2018) 054014 https://doi.org/10.1088/1748-9326/aabb85

Environmental Research Letters

CrossMark

OPEN ACCESS

RECEIVED
4 December 2017

REVISED
16 March 2018

ACCEPTED FOR PUBLICATION
4 April 2018

PUBLISHED
30 April 2018

LETTER

Quantitative attribution of climate effects on Hurricane Harvey's extreme rainfall in Texas

S-Y Simon Wang[1,2], Lin Zhao[3], Jin-Ho Yoon[4,6], Phil Klotzbach[5] and Robert R Gillies[1,2]

1 Utah Climate Center, Utah State University, Logan, UT, United States of America
2 Department of Plants, Soils, and Climate, Utah State University, Logan, UT, United States of America
3 Key Laboratory of Land Surface Process and Climate Change in Cold and Arid Regions, Northwest Institute of Eco-Environment and Resources, Chines Academy of Sciences, Lanzhou, People's Republic of China
4 School of Earth Sciences and Environmental Engineering, Gwangju Institute of Science and Technology, Gwangju, Korea
5 Department of Atmospheric Science, Colorado State University, Ft. Collins, CO, United States of America
6 Author to whom any correspondence should be addressed.

E-mail: yjinho@gist.ac.kr

Keywords: Hurricane Harvey, global warming, downscaling attribution, extreme event

Supplementary material for this article is available online

Abstract

Hurricane Harvey made landfall in August 2017 as the first land-falling category 4 hurricane to hit the state of Texas since Hurricane Carla in September 1961. While its intensity at landfall was notable, most of the vast devastation in the Houston metropolitan area was due to Harvey stalling near the southeast Texas coast over the next several days. Harvey's long-duration rainfall event was reminiscent of extreme flooding that occurred in the neighboring state of Louisiana: both of which were caused by a stalled tropical low-pressure system producing four days of intense precipitation. A quantitative attribution analysis of Harvey's rainfall was conducted using a mesoscale atmospheric model forced by constrained boundary and initial conditions that had their long-term climate trends removed. The removal of the various trends of the boundary and initial conditions minimizes the effects of warming in the air and the ocean surface on Harvey. The 60 member ensemble simulations suggest that post-1980 climate warming could have contributed to the extreme precipitation that fell on southeast Texas during 26–29 August 2017 by approximately 20%, with an interquartile range of 13%–37%. While the attribution outcome could be model dependent, this downscaling approach affords the closest means possible of a case-to-case comparison for event attribution, complementing other statistics-based attribution studies on Harvey. Further analysis of a global climate model tracking Harvey-like stalling systems indicates an increase in storm frequency and intensity over southeast Texas through the mid-21st century.

1. Introduction

Hurricane Harvey made landfall in Texas as a category 4 hurricane on the Saffir–Simpson wind scale and caused at least 73 direct fatalities with an estimated 30 000 people displaced from their homes. The catastrophic flooding produced by Harvey destroyed 9000 homes and damaged 185 000 additional homes (Texas Department of Public Safety). Total economic damage from Hurricane Harvey is estimated at between $90–$160 billion dollars (Blake and Zelinsky 2018). Scientific discussions soon emerged citing that the increased sea surface temperature (SST) in the Gulf of Mexico, the ability of the warmer troposphere to hold more moisture, and the growing stagnation of the atmospheric circulation feasibly, in unison, could strengthen the intensity of Harvey while worsening its impact (e.g. The Guardian, 8/28/2017; Potsdam Institute for Climate Impact Research, 8/28/2017). Subsequent attribution studies indicated an increase in extreme rainfall probability in Texas ranging from 15% (van Oldenborgh *et al* 2017) to 30% (Risser and Wehner 2017) that was linked to anthropogenic warming in the atmosphere, with an associated shortening of return periods for such precipitation events (Emanuel 2017).

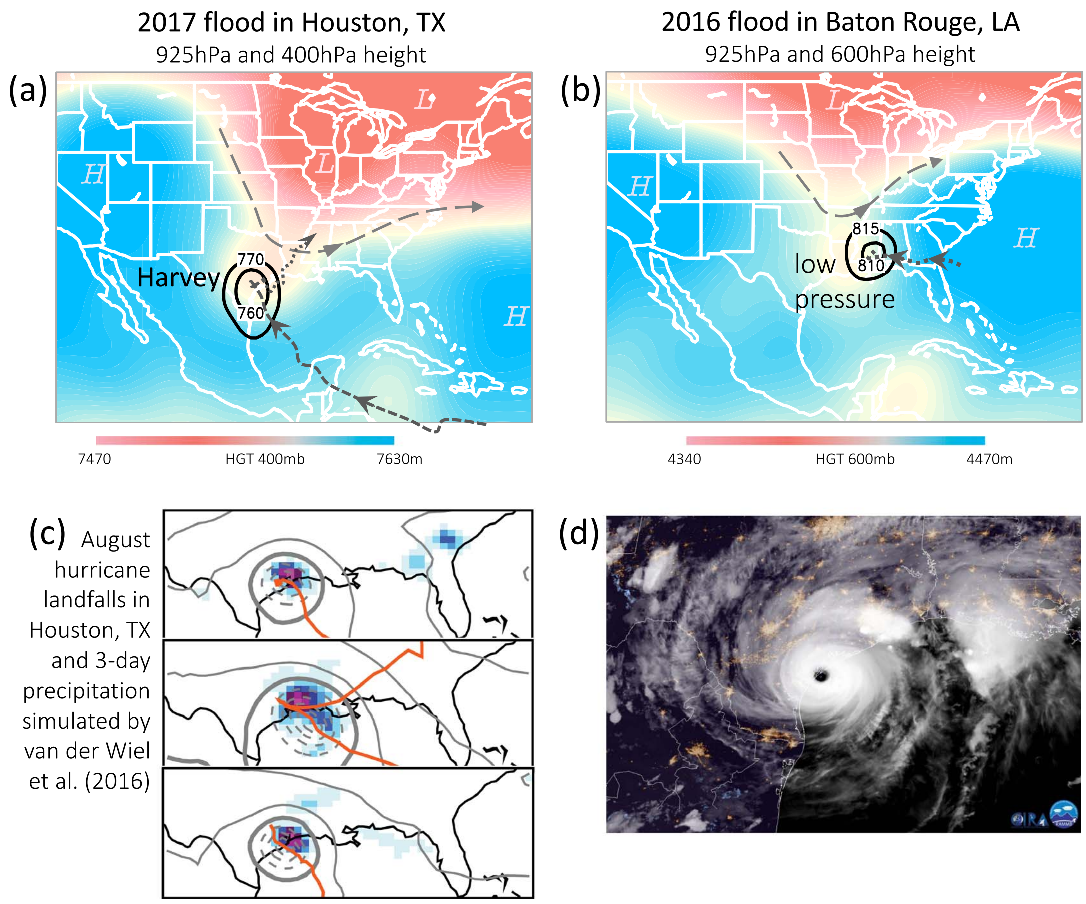

Figure 1. (*a*) Hurricane Harvey on 27 August 2017 and (*b*) the Louisiana storm on 11 August 2016 shown with geopotential height at upper levels (shading) and at 925 hPa (contour) and their tracks as indicated by dashed arrow lines. The approaching synoptic troughs that stalled the storms are outlined by gray lines. (*c*) Adopted and modified from van der Wiel *et al* (2017), the simulated tropical cyclones that resemble Harvey and its associated extreme precipitation in southeast Texas. Data of van der Wiel *et al* (2017) is also available at climexp.knmi.nl/selectfield_att.cgi. (*d*) Satellite image of Harvey making first landfall in Texas (source: Cooperative Institute for Research in the Atmosphere).

Apart from being an intense hurricane, what made Harvey particularly devastating was that the storm stalled near the Texas coast and produced heavy rains for four consecutive days; these were mostly focused on the Houston metropolitan area as the best track shows in figure 1(*a*) (Blake and Zelinsky 2018). The intense rainfall over several days was reminiscent of the Louisiana flood that occurred a year earlier i.e. in August 2016 (figure 1(*b*)). In that event, a stalled low pressure system produced four days of intense rainfall that devastated the city of Baton Rouge (van der Wiel *et al* 2017). The two events bear some resemblance in the time of year that they occurred (August) as well as in their geographical location (neighboring states). Both systems also stalled due to blocking high pressure that prevented movement further inland followed by interactions with a frontal system to the north. In attributing the Louisiana storm of 2016, van der Wiel *et al* (2017) showed that the majority of uppermost extreme precipitation events in the Gulf Coast result from tropical cyclones. The van der Wiel *et al* simulations identified 18 'maximum extreme precipitation events' in the Gulf Coast, each producing a 3 day accumulated rainfall of up to 500 mm. As shown in figure 1(*c*) from van der Wiel *et al* (2017), three of these simulated events resulted from tropical cyclones similar to Harvey.

With the extreme precipitation produced by Harvey and the various rainfall records associated with the storm (see following section), and given the existing literature about the attribution of Atlantic tropical cyclones (van Oldenborgh *et al* 2017), we decided to conduct a quantitative attribution on the impact of long-term climate trends on the heavy precipitation associated with Harvey (which can be linked to both anthropogenic climate change as well as internal decadal variability), through simulations of a regional model forced by various sets of lateral boundary conditions and those with the long-term trends removed. A meteorological overview of Hurricane Harvey is presented in section 2, followed by an explanation of the methodology in section 3. Discussions and a summary are given in sections 4 and 5, respectively.

2. Harvey's meteorological history

Hurricane Harvey was first classified as a tropical depression on 17 August at 6 Z and was upgraded to a tropical storm that same day at 18 Z (Blake and Zelinsky 2018). Strong northeasterly shear, dry air entrainment and rapid storm translation speed contributed to weakening, and Harvey degenerated into an open tropical wave on 19 August while tracking through the eastern Caribbean. After moving across the remainder of the Caribbean and the Yucatan Peninsula as an open wave, Harvey encountered a much more conducive dynamic and thermodynamic environment when it entered the Bay of Campeche. It was upgraded to a tropical depression on 23 August at 12 Z and a tropical storm six hours later. Harvey tracked northward across the Gulf of Mexico and rapidly intensified in an environment of very low vertical wind shear and ∼30 °C sea surface temperatures. During the 48 hour period from 24 August at 0 Z to 26 August at 0 Z, Harvey rapidly intensified by 75 knots. It made landfall shortly thereafter between Port Aransas and Port O'Connor, Texas as a 115 knot category 4 hurricane, with a central pressure at landfall of 937 hPa (figure 1(*d*)). The extreme precipitation that fell on southeast Texas was due to Harvey's stalling characteristics over the next several days—caused by collapsing steering currents. Anomalous high-pressure areas to the northwest and northeast of Harvey resulted in very weak steering over the storm itself (*ref.* steering current—figure 1(*a*)), and Harvey drifted very slowly eastward and then southeastward until it became caught up by a dipping upper-level trough, reversing its track. By 28 August, Harvey had drifted back out over the Gulf of Mexico and continued tracking slowly east-northeastward over the extreme western portion of the Gulf of Mexico over the next two days. By early 30 August, Harvey made its final landfall in Cameron Parish, LA as a weak tropical storm and weakened as it moved further inland (Blake and Zelinsky 2018).

Harvey's landfall ended the longest-running United States major (category 3+) hurricane landfall drought on record that had been ongoing since Hurricane Wilma in 2005 (Hart *et al* 2016). It was the first land-falling category 4 hurricane to hit the state of Texas since Hurricane Carla in 1961. Harvey's landfall pressure of 937 hPa was also the lowest for any hurricane in the Gulf of Mexico hurricane since Rita in 2005. Large parts of the Houston metropolitan area received over 30 inches of rain from Harvey, with a United States record of 60.58 inches recorded in Nederland, Texas. Harvey's proximity to the Gulf of Mexico allowed it to tap into copious amounts of moisture that inundated the Houston metropolitan area triggering catastrophic flooding.

3. Data and modeling approach

3.1. Data sources

Harvey's meteorological history was summarized from the National Hurricane Center best track report (Blake and Zelinsky 2018). Observed precipitation data were derived from the 4 km NCEP Stage-IV Quantitative Precipitation Estimates (Lin and Mitchell 2005). For sea surface temperatures, we used the Extended Reconstructed Sea Surface Temperature (ERSST) version 4. The NCEP-NCAR Reanalysis-1 data (R1) and the NCEP-DOE Reanalysis 2, or R2 (Kanamitsu *et al* 2002) were used to depict the atmospheric variables and to compute the trends. For future climate projections, we analyzed the Community Earth System Model version 1 (CESM1) under the Large Ensemble (LE) Project (Kay *et al* 2015). We used the LE simulations for the 2006–2080 period with RCP8.5 forcing, producing 40 members with selected daily variables at a spatial resolution of 0.9° long. × 1.25° lat.

3.2. Regional model

Simulations using the Advanced Research Weather Research and Forecasting (WRF-ARW) model (Skamarock and Klemp 2008) version 3.8 were performed for the heavy precipitation period over southeast Texas from 0000 UTC 26 August to 0000 UTC 30 August 2017. The model was forced by initial conditions (IC) and lateral boundary conditions (LBC) using the 0.5° × 0.5°-resolution Global Forecast System (GFS) initial analysis. We focused on the post-1980 trend in both tropospheric and ocean surface temperature and conducted four experiments: (1) A control simulation forced by the original GFS analysis as IC and LBC, and a set of 'detrended' simulations in which we removed the linear trends from the IC and LBC for (2) SST (denoted as DSST), (3) all tropospheric variables (DAIR), and (4) both SST and tropospheric variables (DSST+DAIR). The trends were first computed from the R2 monthly data for each variable and then linearly interpolated onto the GFS's resolution and pressure levels. Then, we subtracted these trends from the GFS's initial analysis (geopotential height, horizontal winds, air temperature, etc.) before using it as IC and LBC to drive the WRF-ARW. To evaluate model sensitivity, we also added a double-trend simulation forced by the original LBC to which the post-1980 trends in both the atmosphere and SST were added instead of removed, hence 'doubling' the warming effect; this is denoted as DB runs.

The assumption here is that any post-1980 trend manifest in the troposphere and ocean surface contains signals that are traceable to anthropogenic global warming, which is supported by most attribution analysis (Weaver *et al* 2017). Of course, we also had to assume that Harvey would occur anyway within the climatically detrended environment. This 'detrended

Table 1. Twenty combinations of different cumulus schemes and microphysics in WRF-ARW v3.8 (omitting references due to page limits), which were run at three spatial resolutions of 10, 15 and 20 km.

No	Cumulus schemes	Microphysics
1	Kain–Fritsch	Kessler
2	Betts–Miller–Janjic	Kessler
3	Modifed Tiedtke	Kessler
4	New GFS simplified Arakawa-Schubert	Kessler
5	Kain–Fritsch	Lin
6	Betts–Miller–Janjic	Lin
7	Modifed Tiedtke	Lin
8	New GFS simplified Arakawa-Schubert	Lin
9	Kain–Fritsch	WSM-3
10	Betts–Miller–Janjic	WSM-3
11	Modifed Tiedtke	WSM-3
12	New GFS simplified Arakawa-Schubert	WSM-3
13	Kain–Fritsch	Ferrier (new Eta)
14	Betts–Miller–Janjic	Ferrier (new Eta)
15	Modifed Tiedtke	Ferrier (new Eta)
16	New GFS simplified Arakawa-Schubert	Ferrier (new Eta)
17	Kain–Fritsch	Thompson
18	Betts–Miller–Janjic	Thompson
19	Modifed Tiedtke	Thompson
20	New GFS simplified Arakawa-Schubert	Thompson

downscaling' approach follows that used by Cho *et al* (2016) for the attribution analysis of the June 2013 flood in northern India and the role climate warming played in that event. To assess simulation uncertainty, the WRF-ARW model was run with 60 members in each of the four experiments; these encompass 20 combinations from four microphysics schemes and five cumulus parameterization schemes (listed in table 1) that were run at three spatial resolutions: 15, 20, and 25 km ($4 \times 5 \times 3 = 60$ members). We used a single domain centered around Houston, TX (30°N, 95°W) with the domain outlined in figure 3. To better depict the environmental conditions and associated changes from the detrending, we enabled the '3 dimensional analysis and surface nudging' of WRF-ARW in all of the experiments.

4. Results

4.1. WRF-ARM attribution

In the Gulf of Mexico (defined as 100-80°W, 20–30°N), August SST has warmed by ~0.7 °C since 1980 (figure 2(*a*) red line), while the lower tropospheric temperature within the 1000–500 hPa layer has warmed by 1.4 °C through 2017 (figure 2(*b*), based on R1 data). Precipitable water over the Gulf of Mexico has increased by 7.3% since 1980 with August 2017 being the highest monthly value per R1 data (figure 2(*c*)). In the WRF-ARW detrended experiments (2)–(4), such post-1980 trends were removed from all the meteorological variables in the IC and LBC. We refer to these simply as climate trends rather than global warming trends, since it is likely that not all of the SST increase in the Gulf of Mexico since 1980 is due to anthropogenic causes. The Atlantic Multidecadal Oscillation, for example, has a pronounced signal in the Gulf of Mexico (Enfield *et al* 2001), as is evidenced in the multi-decadal variability of SST (figure 2(*a*)) embedded in the long-term warming trend. On the other hand, the warming after 1990 did start to exceed the spread of variability as shown by the CESM1 historical experiment ensembles in both the SST (figure 2(*d*)) and lower-tropospheric temperature (figure 2(*e*)), suggesting a prominent role of anthropogenic warming.

Harvey produced extremely heavy rainfall in southeast Texas during 26–29 August 2017. The four-day average of 700 h Pa geopotential height and accumulated precipitation from 26–29 August, produced by the control simulation from the ensemble of 60 members, are shown in figure 3(*b*) and are compared with the observed precipitation and the 12 km North American Mesoscale model initial data in figure 3(*a*). The simulated center of Harvey is very close to its actual location but the precipitation centers are shifted about 120 km to the southwest of the observed—a persistent bias. The patterns of accumulated precipitation in DSST, DAIR, DSST+DAIR and DB (figures 3(*c*)–(*f*)) follow the slightly shifted precipitation of the control run and are more concentrated near the hurricane center than the observation (figure 3(*a*)). Nevertheless, the metropolitan area of Houston is within the simulated precipitation maxima indicating that model bias is minimal in our assessment.

The box and whisker diagram in figure 4(*a*) shows the median and spread of the 26–29 August accumulated precipitation *ratio* compared to the observation, averaged over southeast Texas (red box in figure 3). Based on the median, the control precipitation ensemble is only 1% smaller than the observation with an interquartile range from −12% to +8% and we considered this a reasonable simulation. Compared to the control run, the change in the simulated precipitation in southeast Texas was a 3% reduction in DSST, a 17% reduction in DAIR, and a 20% reduction in DSST+DAIR with an interquartile range of 10%–35%. In the double-trend experiment (DB), the precipitation median was increased by 9% with the upper quartile exceeding 20%. Since Harvey lingered along the Gulf Coast through 30 August, we also tested the daily precipitation accumulated through 27–30 August (see supplemental figure S1 available at stacks.iop.org/ERL/13/054014/mmedia). For this later period, the median change was a 9% reduction in DSST, a 22% reduction in DAIR, and a 26% reduction in DSST+DAIR while the DB experiment increased the precipitation by 10%—these are more robust change than from 26–29 August. It is noteworthy in the DSST+DAIR experiment of 27–30 August (figure S1) that even the upper extreme was lower than the observation, implying that climate warming can induce even more precipitation from hurricanes as strong as Harvey.

The impact of the climate trends on Harvey's strength was examined in terms of the central pressure difference from the observation during the 4 day

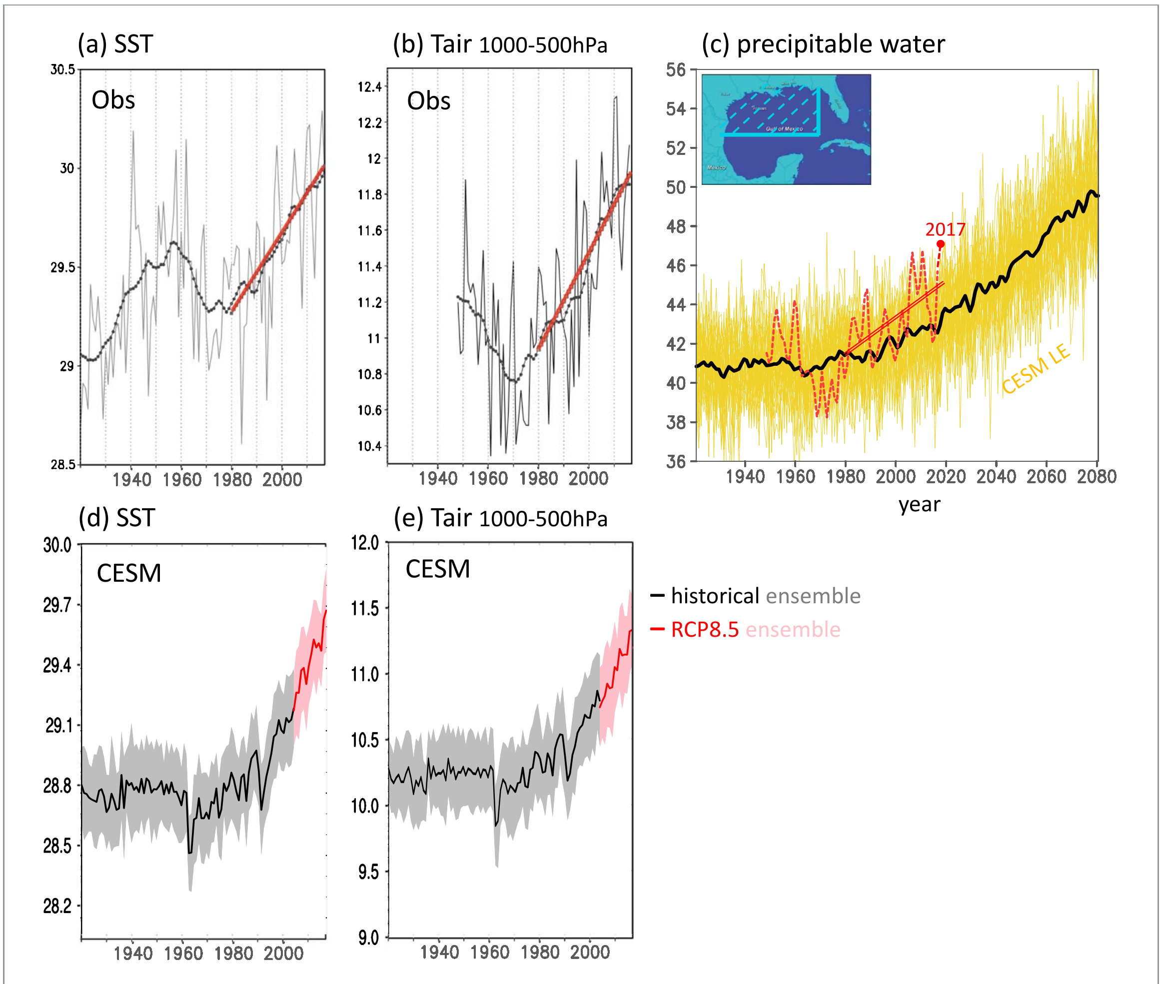

Figure 2. Observed August (*a*) SST and (*b*) air temperature in °C averaged from 1000–500 hPa overlaid with linear trends, as well as CESM LE (yellow) and observed (red) precipitable water over the Gulf of Mexico as outlined by the inset map. Black line in (*c*) is the 30 year running mean. (*d*) and (*e*) Same as (*a*) and (*b*) but from the CESM1 LE data.

period, which is shown in figure 4(*b*). Based on the median, the control run underestimated the center pressure by 2 hPa and DSST increased the pressure slightly from the control run by 0.3 hPa. The differences between control and both DAIR and DSST+DAIR are much more pronounced, increasing the center pressure by 5–6 hPa during 26–29 August (8 hPa during 27–30 August; figure S1). In DB, the center pressure was 2.5 hPa lower than the observed while the lower quartile was 6 hPa lower, suggesting that additional SST warming could intensify future Harvey-like hurricanes even further. The daily breakdown of these precipitation and central pressure comparisons is displayed in supplemental figure S2; the reduction effects of DAIR and DSST+DAIR had on Harvey's precipitation and central pressure are consistent. These results uniformly indicate the strengthening effect of the climate trends on Harvey.

Notable is the impact of DAIR on Harvey's precipitation and intensity which is much stronger than that of DSST, implying that climate trends in the atmospheric BC are critical in influencing Harvey. To infer the possible physical processes involved, we examined the post-1980 trends in the 300 hPa and 900 h Pa geopotential height, shown in supplemental figures S3(*a*) and S3(*b*). The increased upper-level height accompanying the decreased low-level height suggests an increase in the atmospheric thickness, likely associated with the mid-level warming; this is shown to be the case by a significant positive air temperature trend at 500 hPa (figure S3(*c*)). Such an increase in the atmospheric thickness and mid-tropospheric warming coincides with the vertical structure of a developing tropical cyclone which can be found on www.usno.navy.mil/NOOC/nmfcph/RSS/jtwc/pubref/References/GUIDE/chap4img/fig402.jpg and arguably contributes to the intensification of hurricanes.

4.2. Projection of the stalled storm

What is displayed in figure 1(*a*) describes an encounter between two sub-synoptic weather systems moving in opposite directions over Texas. Such weather systems are not uncommon but are random in nature. A case such as this fits the description of a classic tropical-extratropical interaction that combines abundant moisture carried with the low-pressure system and a vorticity source associated with the upper trough. Like the 2016 stalled cyclone that inundated portions of Louisiana (figure 1(*b*)), the upper trough moving through the central US induced a positive vorticity

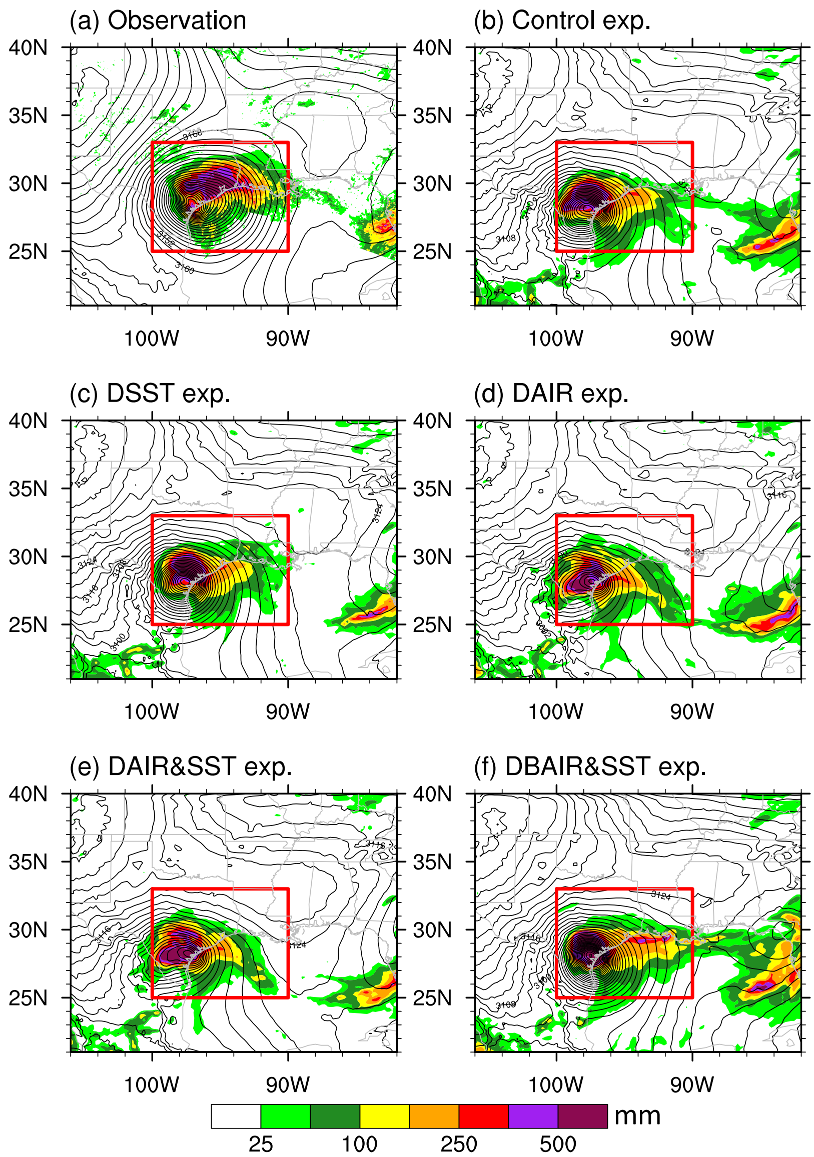

Figure 3. 26–29 August average of 700 hPa geopotential height (contour) and precipitation (shading) from (*a*) the observations of NAM initial and Stage IV and from the ensembles of (*b*) control, (*c*) DSST, (*d*) DAIR, (*e*) DAIR+DSST, and (*f*) double-trend/DB experiments. The red box is used for the domain average shown in figure 4.

tendency that intercepted the low-pressure system, inducing vortex stretching in the lower levels (Wang *et al* 2016). To provide a synoptic perspective, we tracked similar weather systems that resembled the unusual encounter of Harvey and the approaching cyclone that stalled it. A similar analysis was done by Wang *et al* (2016) for the August 2016 Louisiana stalled cyclone, and the ensuing analysis follows their method.

To identify similar cases involving a stalled storm along the Gulf Coast interacting with a dipping synoptic trough from the north, we conducted the analysis based upon the 26–29 August average conditions. We applied a spatial harmonic analysis to the four day geopotential height at 850 hPa to filter out zonal wavenumbers 8 and beyond, based upon the size of landfalling Harvey (~15° longitude in diameter); this spatial filter isolated the stalled Harvey as a low-pressure anomaly while eliminating ambient large-scale circulations such as the Bermuda High. We then applied a low-pass filtering for the 300 h Pa geopotential height by retaining wavenumbers 1–8; this was to depict the synoptic-scale flow pattern consisting of the western ridge and the eastern trough flow pattern, like the synoptic setting shown in figure 1(*a*), while removing shorter waves. This spatial filtering analysis was applied to both the R2 and CESM1 data.

Next, to objectively assess the extent to which any historical and simulated storm compares with Harvey, we adopted the 'pattern correlation coefficient' that calculates the Pearson product-moment coefficient of linear correlation between two variables at corresponding locations; this method outputs a single number (correlation coefficient denoted as ρ_P) that conveniently depicts the similarity between two systems. We computed ρ_P of the R2 geopotential height during 26–29 August with any four day mean of the

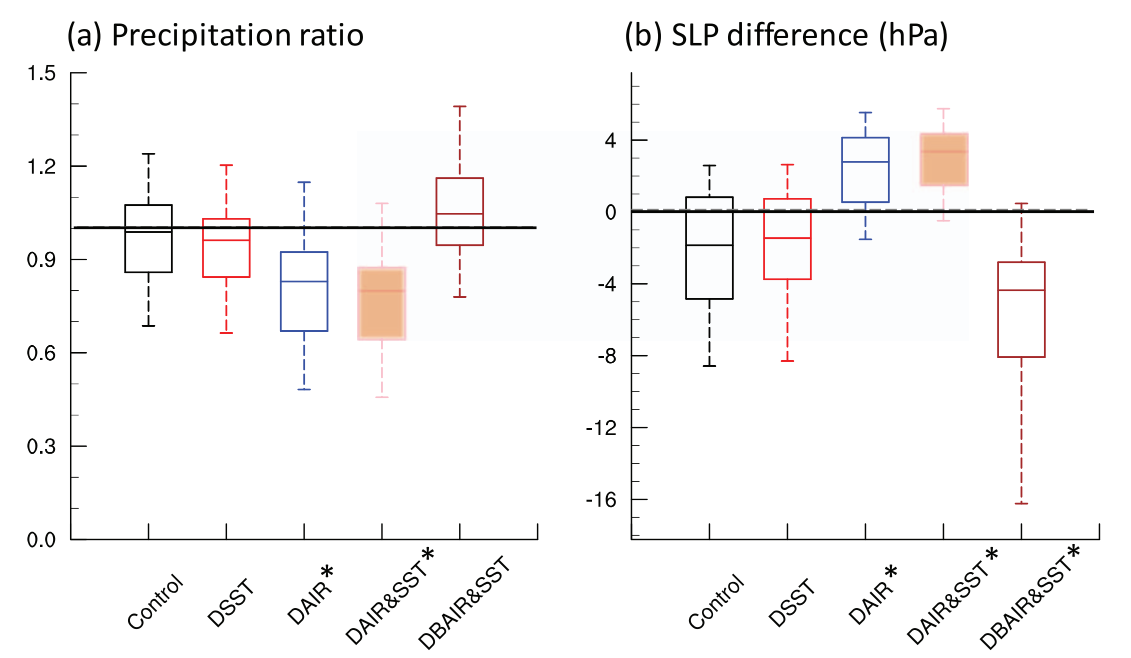

Figure 4. Box and whisker plots of (*a*) the ratio of simulated precipitation and (*b*) minimum sea level pressure relative to the observation with 60 ensemble members each, derived from (left to right) control, DSST, DAIR, DAIR+DSST (color filled), and DB runs. The *x*-axis labels marked with * indicate a significant difference from control runs at 95% confidence interval per *t*-test.

CESM1 LE, after applying the spatial filtering described above to both geopotential height fields. The comparison was made for two domains, a synoptic one for the upper level with low-pass filtering (*ref.* steering conditions and stagnation associated with the low-pressure system in question). It is expected that there would be a range of cases from 'somewhat similar' to 'almost identical' in the historical and simulated data; thus, we designated a range of ρ_P from a low bar of 0.5 (somewhat similar) as the minimal criterion to a high bar of 0.8 (almost identical) with a 0.05 increment for both pressure levels; this led to 49 combinations with seven ρ_P intervals in the upper level pairing to seven ρ_P intervals in the lower level. Furthermore, we applied an intensity criterion using the minimum central value of the 850 h Pa geopotential height. In any 4 day sequence, the daily minimum height within the low-pressure system over southwest Texas (red box in figure 3) had to be at least 0.6 of the value exhibited during 26–29 August 2017. An evaluation made between the reanalysis data and the CESM1 Historical LE yielded a roughly 1:2 ratio of identified cases (not shown). The higher number of cases in CESM1 is expected due to the low-bar criteria that includes extra weaker cases.

The temporal distribution of the identified cases during the 2006–2080 period is presented as a series of box plots in figure 5(*a*) for the number of cases, and in figure 5(*b*) for the four day accumulated precipitation (including all 49 ρ_P combinations per year from each member). A 15 year running mean of their medians is also shown. There is an apparent increase in the number of cases beginning in ~2050, and this is concurrent with event precipitation increases that are projected to continue to ~2070. The Atlantic Ocean has been projected to feature an overall increase in intense tropical cyclone frequency (Jones *et al* 2016), with more category 4–5 storms and fewer weaker storms (Bender *et al* 2010, Knutson *et al* 2010). A warming tropical Atlantic Ocean can induce low-pressure anomalies over the Gulf of Mexico during late summer (Weaver *et al* 2009) and subsequently enhance the conditions for tropical cyclone formation. However, we note that the ability of CESM1 to simulate and project tropical cyclones is unclear, and we do not have a definitive explanation for the subsequent decline after 2070 other than referring it to internal variability. Likewise, the 2050–2070 increase also could be due to internal variability, though the overall uptrends in precipitation and case number from 2020 to 2080 are arguably attributable to climate warming. Here, as was the case in the WRF-ARW simulations, we caution that the projection results in figure 5 may differ by model and by the physics schemes used.

5. Discussion

The reason for the increasing number of low-pressure systems in the Gulf Coast (figure 5(*a*)) is manifold, involving both natural and anthropogenic origins. Some modeling studies project that North Atlantic category 4–5 storms will increase (Bender *et al* 2010, Knutson *et al* 2013) while weaker hurricanes will likely decrease (Jones *et al* 2016). To our knowledge, no studies have focused specifically on future tropical cyclone strength in the Gulf of Mexico, except for a loose comparison made in van der Wiel *et al* (2017). Given

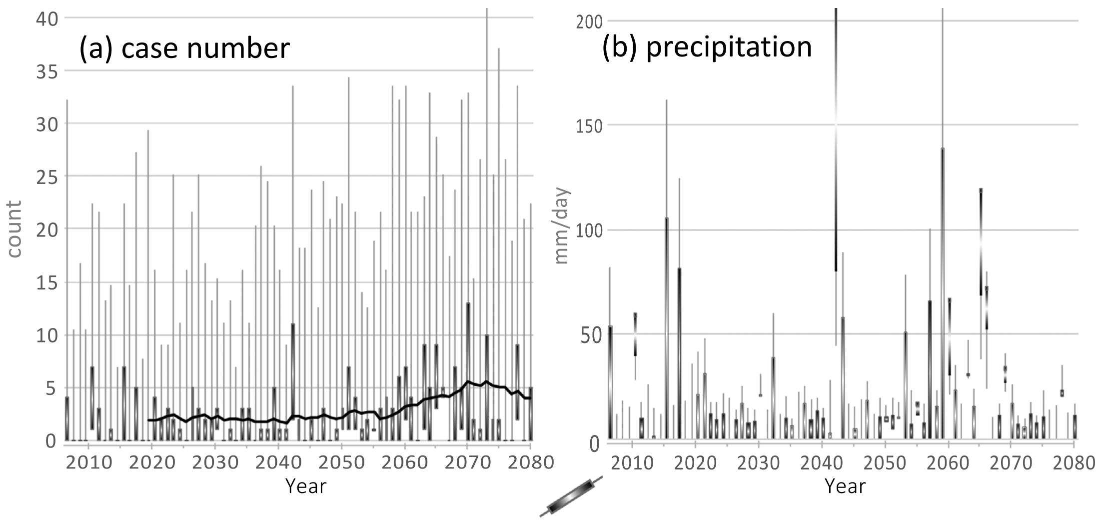

Figure 5. Box and whisker plots of (*a*) the case number accumulated and (*b*) event precipitation averaged over southeast Texas of Harvey-like weather systems depicted from the CESM LE projection data from the ensemble of 40 members for each year. The medians are connected by thick solid line by the backward 15 year moving average.

the widened increase in the number of cases (figure 5(*a*)) between low-bar criteria and high-bar criteria, it is possible that the increase in storm precipitation is mainly driven by weaker tropical cyclones in the Gulf of Mexico.

High moisture content in the atmosphere plays an important role in strong hurricanes like Harvey as well as the storms leading to the 2016 Louisiana flood (Wang *et al* 2016). Precipitable water in the Gulf of Mexico has increased considerably and will only increase in a warming climate; this was both observed and projected by CESM1 as shown in figure 2(*c*). Consequently, the prospect of future tropical cyclones resulting in extreme precipitation is a scenario that the Gulf Coast and coastal metropolitan areas will likely face in the future, and the simulation results of figure 5(*b*) also suggest it. Nonetheless, recent climate projection studies (Gao *et al* 2012, Janssen *et al* 2014, Wuebbles *et al* 2014) did not underscore the Gulf States as a hotspot for a significant increase in summertime extreme precipitation. High-emission climate projections showed only a weak increase in the maximum daily precipitation in Texas and Louisiana, considerably less than the northeast US and Midwest (Wuebbles *et al* 2014); this apparent discrepancy between the two projections requires caution in interpretation.

Conceptually, our approach that constrains the boundary and initial conditions of an atmospheric model used to create a synoptic event is in line with the emerging 'storyline approach' of attribution analysis (Zappa and Shepherd 2017). When it comes to attribution analysis, the mere use of observational data and model free runs is not adequate enough to reach robust conclusions. Global model free runs may approximate a historical hurricane, e.g. as in the Hurricane Sandy attribution (Lackmann 2015), but they do not necessarily replicate the environmental conditions associated with the particular storm. Using the dynamical downscaling approach forced by observed IC and LBC provides the closest possible influences of the true environmental conditions at the time of a mesoscale or weather system of interest. While the simulations suggest that Harvey's precipitation over southeast Texas as well as its intensity could have been enhanced by climate warming trends, we acknowledge that the estimate can change depending on a number of factors, such as different models used and their settings, different IC and LBC sources, and choice of trend periods removed.

6. Conclusion

While the Gulf Coast is no stranger to strong hurricanes, a tropical cyclone that stalls for days over a major metropolitan area and results in excessive rainfall is a recipe for disaster. Quantitative attribution conducted by WRF-ARM downscaling simulations, with the climate trends removed from the IC and LBC, suggest that post-1980 warming in both the ocean and atmosphere likely resulted in a ∼20% increase of the accumulated event precipitation with an interquartile range of 13%–37%. Preliminary CESM1 analysis projecting stalled storms over southwest Texas, in conjunction with recent analyses of a similarly stalled storm in Louisiana (van der Wiel *et al* 2017, Wang *et al* 2016), signifies an increasing trend in the number of cases that have similar synoptic patterns and associated stationarity to that of Harvey. Precipitation associated with these stalled storms was also projected to increase, despite CESM1's relatively coarse resolution prevents a more quantitative assessment.

The method demonstrated here echoes one of the alternative ways outlined in Trenberth *et al* (2015) to resolve the challenge facing attribution analysis from a physical standpoint, that is, questioning whether observed changes in the thermodynamic state affected the impact of a particular event. We note that the post-1980 warming is not simply due to anthropogenic causes but also likely involves natural climate variability and random weather systems. Risser and Wehner (2017) conducted extreme value analysis using CO_2 concentration and annually-averaged El Niño–Southern Oscillation (ENSO) as covariates and found that human-induced climate change likely increased Harvey's precipitation in the Houston metropolitan area by 40% with a lower bound estimate of 18%. We note, however, similarly to what they acknowledged in their paper, that other natural modes of variability such as the AMO may be responsible for some of the increase in SST in the Gulf of Mexico. In the context of event attribution, our regional downscaling attribution approach went one step further in conducting a more direct, 'apples-to-apples' comparison of Harvey's extreme precipitation when compared to the value-based (not event-specific) statistical analysis or return period analysis that relies on capturing similar 'Harvey-like' events, without dealing with the environment factors and synoptic settings accompanying the particular event of interest. In general, our result is in agreement with that of van Oldenborgh *et al* (2017) and Emanuel (2017) in that anthropogenic warming in the atmosphere contributed to the rainfall intensity of Harvey and may lead to more frequent similar storms in the future.

The estimate from the present downscaling attribution is by no means absolute and attributing convectively-driven extreme precipitation events is challenging. Our purpose here is not necessarily to provide a definitive number but rather to propose a way to provide a more direct, quantitative measure for conducting extreme precipitation event attribution. For a better representation of storm-scale structures in organized convective systems, the US Climate Variability and Predictability Program (CLIVAR) suggest future research to consider utilizing convective permitting modeling that shows superior performance in warm-season convection (US_CLIVAR 2017). We thus call for a careful reevaluation of the projection of both tropical cyclones and other convective systems that may become more stalled in the future and produce more rainfall.

Acknowledgments

S W was supported by the SERDP grant RC-2709. J Y was supported by the GIST Research Institute (GRI) Grant funded by the GIST in 2018. P K would like to acknowledge funding from the G Unger Vetlesen Foundation.

ORCID iDs

Jin-Ho Yoon https://orcid.org/0000-0002-4939-8078

References

Bender M A, Knutson T R, Tuleya R E, Sirutis J J, Vecchi G A, Garner S T and Held I M 2010 Modeled impact of anthropogenic warming on the frequency of intense Atlantic hurricanes *Science* **327** 454–8

Blake E S and Zelinsky D A 2018 *National Hurricane Center Tropical Cyclone Report: Hurricane Harvey* (Miami, FL: N H Center) p 76

Cho C, Li R, Wang S-Y, Yoon J-H and Gillies R R 2016 Anthropogenic footprint of climate change in the June 2013 northern India flood *Clim. Dyn.* **46** 797–805

Emanuel K 2017 Assessing the present and future probability of Hurricane Harvey's rainfall *Proc. Natl Acad. Sci.* **114** 12681–4

Enfield D B, Mestas-Nuñez A M and Trimble P J 2001 The Atlantic Multidecadal Oscillation and its relation to rainfall and river flows in the continental US *Geophys. Res. Lett.* **28** 2077–80

Gao Y, Fu J, Drake J, Liu Y and Lamarque J 2012 Projected changes of extreme weather events in the eastern United States based on a high resolution climate modeling system *Environ. Res. Lett.* **7** 044025

Hart R E, Chavas D R and Guishard M P 2016 The arbitrary definition of the current Atlantic major hurricane landfall drought *Bull. Am. Meteorol. Soc.* **97** 713–22

Janssen E, Wuebbles D J, Kunkel K E, Olsen S C and Goodman A 2014 Observational-and model-based trends and projections of extreme precipitation over the contiguous United States *Earth's Future* **2** 99–113

Jones J J, Stephenson T S, Taylor M A and Campbell J D 2016 Statistical downscaling of North Atlantic tropical cyclone frequency and the amplified role of the Caribbean low-level jet in a warmer climate *J. Geophys. Res.: Atmos.* **121** 3741–58

Kanamitsu M, Ebisuzaki W, Woollen J, Yang S-K, Hnilo J J, Fiorino M and Potter G L 2002 NCEP–DOE AMIP-II Reanalysis (R-2) *Bull. Am. Meteorol. Soc.* **83** 1631–43

Kay J *et al* 2015 The community earth system model (CESM) large ensemble project: a community resource for studying climate change in the presence of internal climate variability *Bull. Am. Meteorol. Soc.* **96** 1333–49

Knutson T R *et al* 2010 Tropical cyclones and climate change *Nat. Geosci.* **3** 157–63

Knutson T R *et al* 2013 Dynamical downscaling projections of twenty-first-century Atlantic Hurricane activity: CMIP3 and CMIP5 model-based scenarios *J. Clim.* **26** 6591–617

Lackmann G M 2015 Hurricane Sandy before 1900 and after 2100 *Bull. Am. Meteorol. Soc.* **96** 547–60

Lin Y and Mitchell K E 2005 The NCEP Stage II/IV hourly precipitation analyses: development and applications *19th Conf. on Hydrology, American Meteorological Society* paper 1.2

Risser M D and Wehner M F 2017 Attributable human-induced changes in the likelihood and magnitude of the observed extreme precipitation during Hurricane Harvey *Geophys. Res. Lett.* **44** 12,457–64

Skamarock W C and Klemp J B 2008 A time-split nonhydrostatic atmospheric model for weather research and forecasting applications *J. Comput. Phys.* **227** 3465–85

Trenberth K E, Fasullo J T and Shepherd T G 2015 Attribution of climate extreme events *Nat. Clim. Change* **5** 725

US_CLIVAR 2017 US CLIVAR Summit Report 38 (https://doi.org/10.5065/D5066CJ5068C5064)

van der Wiel K *et al* 2017 Rapid attribution of the August 2016 flood-inducing extreme precipitation in south Louisiana to climate change *Hydrol. Earth Syst. Sci.* **21** 897–921

van Oldenborgh G J *et al* 2017 Attribution of extreme rainfall from Hurricane Harvey, August 2017 *Environ. Res. Lett.* **12** 124009
Wang S-Y, Zhao L and Gillies R R 2016 Synoptic and quantitative attributions of the extreme precipitation leading to the August 2016 Louisiana flood *Geophys. Res. Lett.* **43** 11,805–814
Weaver S J, Schubert S and Wang H 2009 Warm season variations in the low-level circulation and precipitation over the Central United States in observations, AMIP simulations, and idealized SST experiments *J. Clim.* **22** 5401–20
Weaver S J, Kumar A and Chen M 2017 Recent increases in extreme temperature occurrence over land *Climate Extremes* (New York: Wiley) pp 105–14
Wuebbles D J *et al* 2014 CMIP5 climate model analyses: climate extremes in the United States *Bull. Am. Meteorol. Soc.* **95** 571–83
Zappa G and Shepherd T G 2017 Storylines of atmospheric circulation change for european regional climate impact assessment *J. Clim.* **30** 6561–77

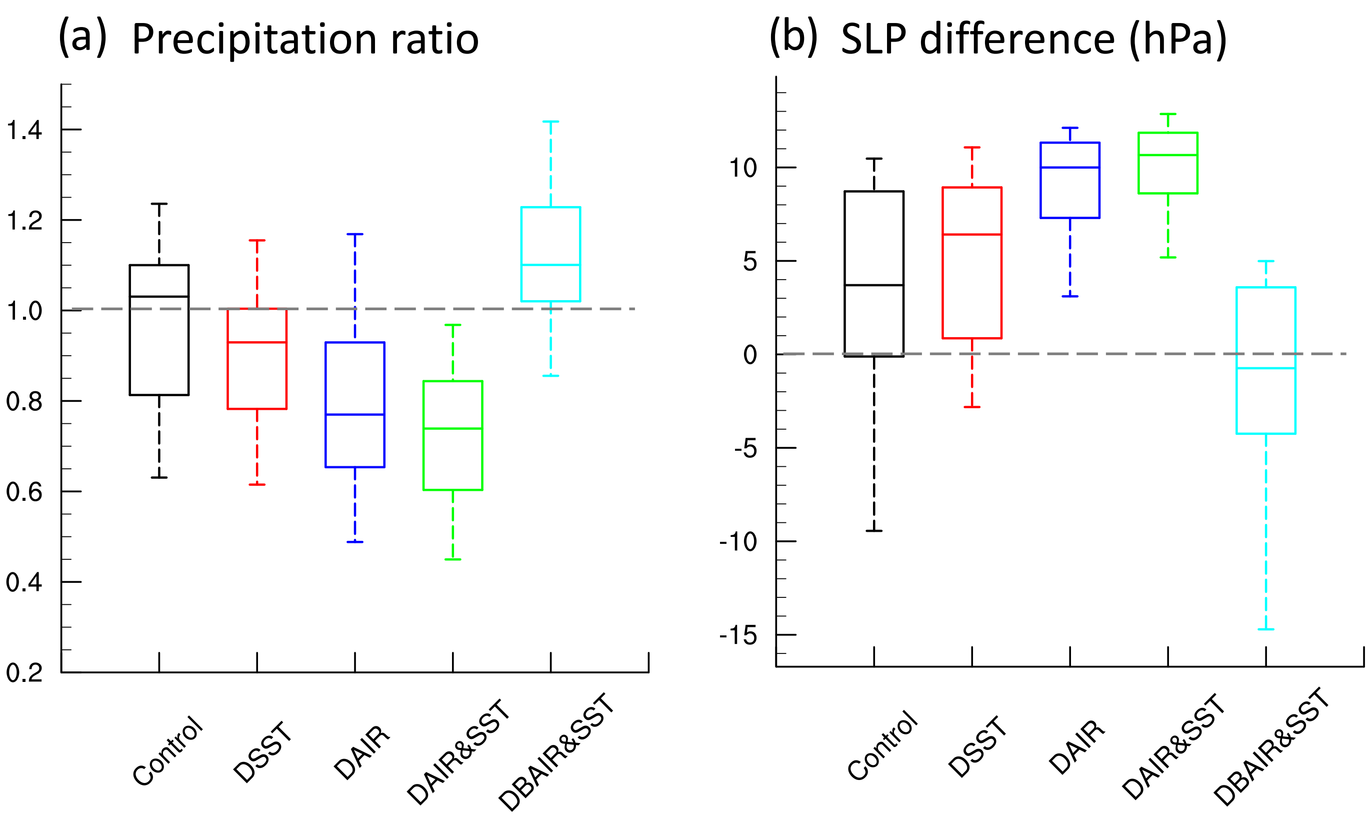

Supplemental Figure S1

Same as Fig. 4 but for the period of 27-30 August 2017.

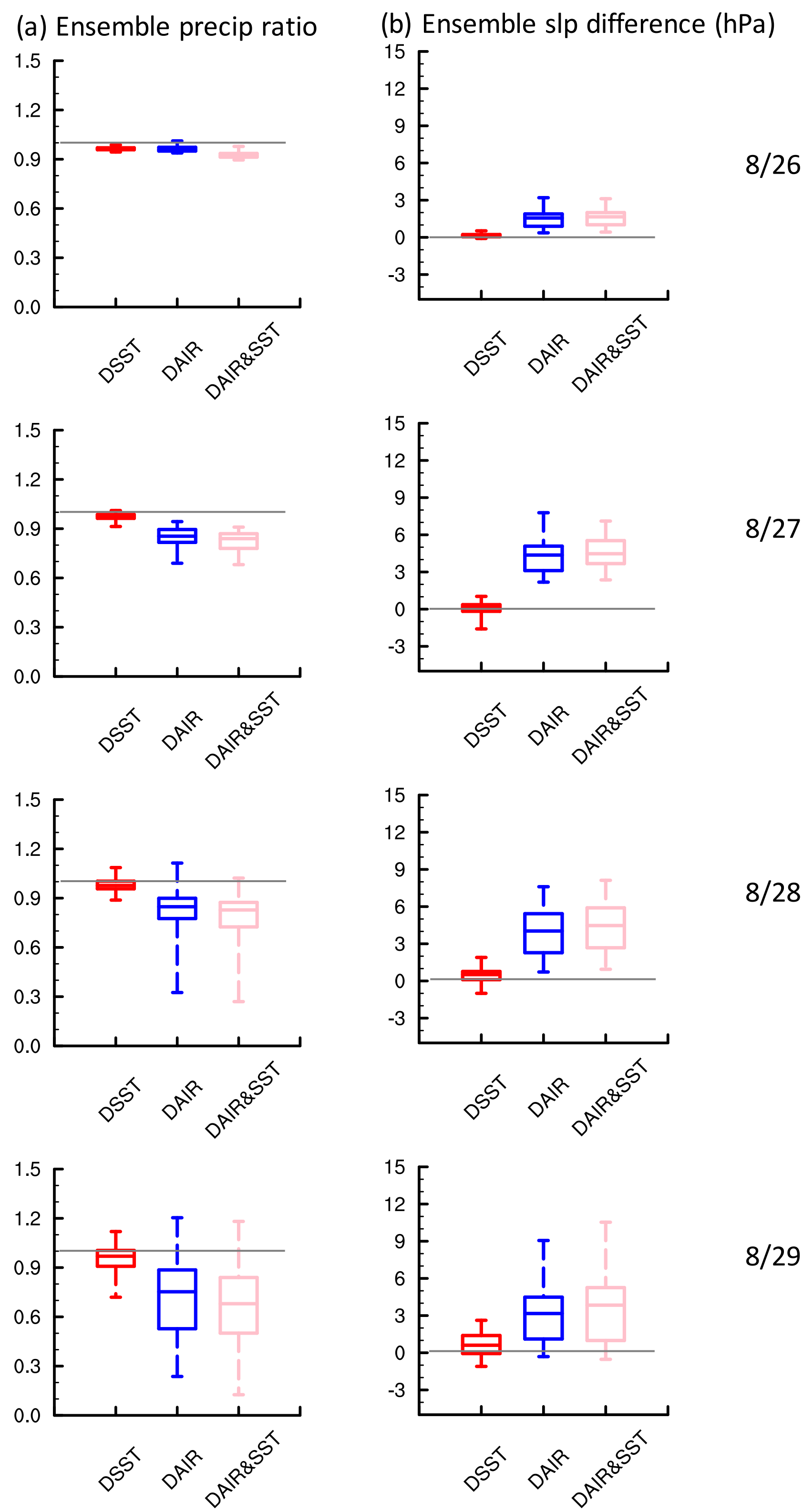

Supplemental Figure S2

Similar to Fig. 4 but showing only the ratio between the experiments displayed and the control run on each day of 26-29 August 2017.

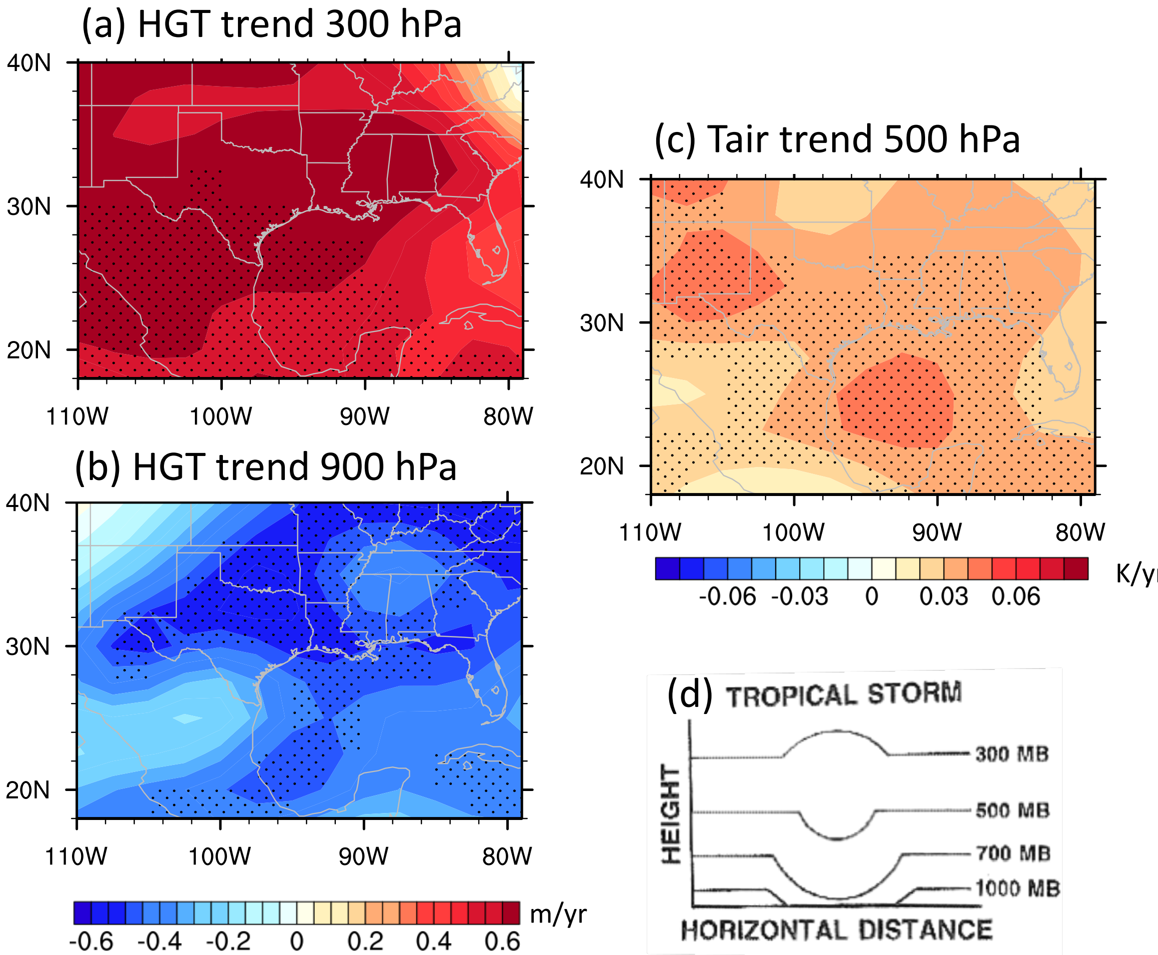

Supplemental Figure S3

Poste-1980 trends in the August (a) 300-hPa and (b) 900-hPa geopotential height and (c) 600-hPa air temperature. Dotted areas indicate significance at 95% confidence interval per Student's *t*-test. These are compared to (d) idealized vertical cross section of a tropical cyclone showing the vertical depth increase as it intensifies. (Source: http://www.usno.navy.mil/)

water

MDPI

Article

Synoptic and Climate Attributions of the December 2015 Extreme Flooding in Missouri, USA

Boniface Fosu[1] and S.-Y. Simon Wang[1, 2] and Kathleen Pegion[3]

[1]Department of Plants, Soils and Climate, Utah State University, Logan, Utah, USA
[2] Utah Climate Center, Utah State University, Logan, Utah, USA
[3] Department of Atmospheric, Oceanic, and Earth Sciences and & Center for Ocean-Land-Atmosphere Studies, George Mason University, Fairfax, Virginia, USA
Received: date; Accepted: date; Published: date

Abstract: Three days of extreme rainfall in late December 2015 in the middle of the Mississippi River led to severe flooding in Missouri. The meteorological context of this event was analyzed through synoptic diagnosis into the atmospheric circulation that contributed to the precipitation event's severity. The midlatitude synoptic waves that induced the extreme precipitation and ensuing flooding were traced to the Madden Julian Oscillation (MJO), which amplified the trans-Pacific Rossby wave train likely associated with the strong El Niño of December 2015. Though the near historical El Niño contributed to a quasi-stationary trough over the western U.S. that induced the high precipitation event, an interference between the MJO and El Niño teleconnections resulted in a relatively weak atmospheric signature of the El Niño in comparison to that of the MJO. The influence of anthropogenic climate change on the relationship between ENSO and precipitation across several central U.S. states was also investigated using 17 CMIP5 models from the historical single-forcing experiments. A regime change in ENSO-related precipitation anomalies appears to have occurred, from being negatively correlated before 1950 to positive and significantly correlated after 1970, suggesting a likely effect of anthropogenic warming on the December 2015 extreme precipitation event.

1. Introduction

During late December 2015, a low-pressure system moved ashore onto the West Coast of the United States and later tracked northeastwards. This trough system induced a strong band of thunderstorms across the U.S. Central and Southern Plains, bringing unseasonably numerous tornadoes and unprecedented flooding (Fig. 1a). The storm and its aftermath caused 50 fatalities and an estimated $3 billion damages in 13 U.S. states, with Missouri being the most impacted by flooding (USGS Report, Holmes et al. 2016). Several antecedent factors contributed to the severity of the flooding in Missouri: First, soil moisture conditions were saturated (Fig. 1b) due to a consistently wet year with record rainfall in November (Fig. 1c). Statewide precipitation was 300% of normal, making it the second wettest December on record and the wettest since 1982 (Fig. 1d). The soil conditions exacerbated the effect of the widespread rains received in December (not shown), before the late-December storm dropped about eight inches of precipitation. The atypical nature of the flooding is further highlighted by the time of year it occurred, since major precipitation and flooding events along the Mississippi River and Missouri have historically taken place in spring or summer (e.g. Hirschboeck 1991, USGS flood reports).

The persistent synoptic patterns associated with the flooding (Fig. 1a) seems to suggest a modulation effect from large-scale circulation anomalies. During December 2015, the El Niño Southern Oscillation (ENSO) was at a near record positive phase, and it is well known that ENSO and its teleconnection can modulate the frequency of wintertime extremes in the U.S. (e.gs Higgins et al. 2000, Schubert et al. 2008). Coincidentally, a mature Madden Julian Oscillation (MJO) episode developed in December and appears to have interfered constructively with the El Niño effect (Fig. S1a). As the primary source of intraseasonal variability in the Earth's climate system (Zhang 2005), the MJO's modulation of tropical convection can initiate poleward propagating Rossby waves that impact extratropical weather patterns and, in turn, influence the leading modes of low-frequency northern hemisphere variability, particularly in the Boreal winter (Riddle et al. 2013, Rodney et al. 2013).

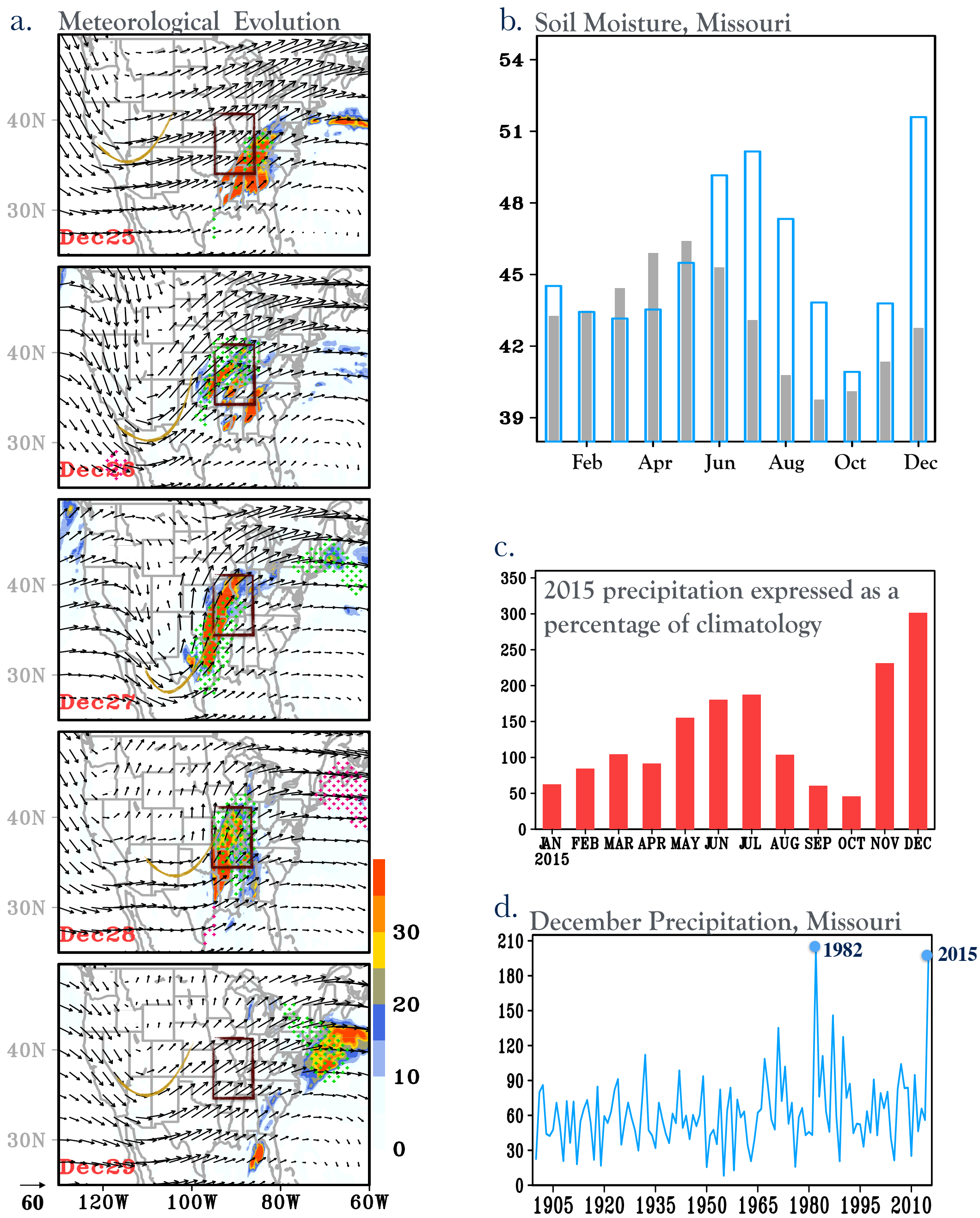

Figure 1

a. Meteorological evolution of the late December event: 250-hPa winds (vectors) and precipitation (mm, shading), from 25–29 Dec 2015. Areas of positive (negative) vertically integrated (from 1000-300 mb) moisture flux convergence greater than $3x10^{-4}$ kgs^{-1} are represented by magenta (green) stipplings. Upper-level short wave troughs are marked with yellow curves. The dark red box delineates the most affected storm areas, i.e. the study region. **b.** 2015 monthly soil moisture (blue outline) (cm) in comparison to the 1950-2010 climatology (gray bars). **c.** Monthly precipitation in 2015 expressed as a percentage of climatology. Each bar is representative of the total precipitation in each month of 2015 expressed as a percentage of that month's climatology. **d.** Interannual variation of statewide monthly precipitation for December for Missouri

Against this backdrop, the purpose of this study is to evaluate the extent to which large-scale circulation patterns associated with the El Niño and MJO may have facilitated the late-December 2015 extreme precipitation in Missouri. What's more, recent studies have reported that the ENSO teleconnection has enhanced under a warming climate, along with its impacts on the southern and central U.S. (Meehl et al. 2007, Stevenson et al. 2012, Wang et al. 2015). In view of this, we also investigate changes in ENSO-related precipitation across the central U.S. (with emphasis on West-North Central and the Southern Plains), particularly when forced by greenhouse gases and deduce the contribution of such changes to the severity of the 2015 Missouri flooding.

The rest of the paper is structured as follows: in Section 2, we outline the methods used to align the typical MJO phase with this case in December 2015, as well as the approach used for assessing the role of the El Niño teleconnection. We move on to results and discussions in Section 3, and provide some concluding remarks in Section 4.

2. Data and Methodology

2.1 Data sources

The Climate Prediction Center's (CPC) model-calculated monthly soil moisture at 0.5° grid spacing is used to estimate monthly soil moisture anomalies (Fan and van den Dool, 2004). For precipitation, we utilize the CPC morphing technique (CMORPH, Joyce et al. 2004) and the Parameter-Elevation Regressions on Independent Slopes Model (PRISM, Daly et al. 2008) datasets for daily and monthly fields respectively. To analyze atmospheric circulation, output from the National Centers for Environmental Prediction/National Center for Atmospheric Research (NCEP/NCAR) global reanalysis at 2.5-degree resolution is used (Kalnay et al. 1996).

Attribution analysis is carried out by assessing long-term changes to ENSO's teleconnection impact on precipitation across the central U.S. using 17 models from phase 5 of the Coupled Model Intercomparison Project (CMIP5). We specifically analyze two historical single-forcing experiments, i.e. the natural-only forcing (NAT) and the greenhouse gas (GHG)-only forcing (Taylor et al. 2011). Each experiment produced multiple members initialized from a long-stable preindustrial (1850) control run up to 2005. Table S1 in the supporting information provides the full name, institute, ensemble size, and spatial resolution of each model.

2.2 Determining relevant MJO phases

The MJO has often been identified by use of an empirical orthogonal function (EOF) analysis. In this study, the state of the MJO is defined by projecting daily anomaly data onto the leading pair of empirical orthogonal functions (EOFs) of equatorially averaged (15^{o}S-15^{o}N) 200 hPa velocity potential (χ_{200}) fields. The EOF analysis covers a three months' period (Dec 1 - Feb 28), and is performed on yearly basis, i.e. from 1979 to 2015. Prior to the EOF computation, χ_{200} is bandpass filtered to the intraseasonal period of 30-60 days to isolate the MJO signal, a method dating back to several MJO studies. The MJO can also be viewed in a two-dimensional phase space defined by the two-leading pair of principal component (PC) from the EOF analysis. Since the phase space diagram is a method to observe both the amplitude and the phase of the MJO during its propagation, we construct yearly phase space diagrams and use them to identify "MJO activity days," defined as days when the MJO amplitude ($i.e. \sqrt{\mathrm{PC1}^2 + \mathrm{PC2}^2}$) is greater than or equal to one (Zhou et al. 2012). Note that before the phase space diagrams are constructed, the two PCs are normalized with their respective mean and standard deviation (Kiladis et al. 2014).

This approach generally follows the methodology of Wheeler and Hendon 2004 (WH04), but unlike WHO4, we use velocity potential (χ_{200}) for the EOF representation instead of a combination of OLR, 850-hPa zonal wind (u850) and 200-hPa zonal wind (u200). Ventrice et al. 2013 shows that OLR is a relatively noisy field both spatially and temporally, with variability mostly limited to the Eastern Hemisphere. Additionally, the inverse Laplacian used to calculate χ_{200} acts as a smoother, which makes χ_{200} more sensitive to global-scale variations of divergence rather than being concentrated on the Indo-Pacific warm pool like OLR.

2.3 Synoptic attribution methods

This section outlines the attribution methods employed to assess the relative contributions of the MJO and El Niño to the synoptic conditions associated with the late December 2015 extreme rainfall, and subsequent flooding in Missouri. This is quite a lengthy section but is necessary to properly interpret the ensuing results from our diagnostic methods.

a. The 2015 December MJO episode

First, the spatial representation and evolution of the MJO event during which the late December 2015 Missouri flooding occurred is constructed. For the remainder of this paper, we call this MJO event the "December MJO episode." In accordance with the phase space diagram for year 2015, the spatial evolution of the December MJO episode is developed by averaging all MJO activity days (*i.e. amplitude* ≥ 1) in each given phase. This is done for both 200 hPa velocity potential (χ_{200}) and streamfunction (ψ_{200}) over a domain spanning the globe longitudinally and from latitude 40°S-80°N. Both χ_{200} and ψ_{200} are bandpass-filtered within a 30-60 day intraseasonal frequency.

Next, we take an approach based on the idea that the contribution of the December MJO episode to the synoptic conditions that caused the Missouri flooding can statistically be separated. This can be achieved through regression analysis that involves an "MJO phase composite" comprising past MJO events with identical characteristics to the December 2015 MJO episode. In line with this, 36 MJO episodes before 2015 are constructed on yearly basis, from 1979 to 2014 by following the initial steps outlined above. The so-called MJO phase composite is created from these 36 MJO episodes. But before the composition is done, we take measures to ensure that the eight phases of the MJO phase composite can correctly align with the corresponding phases of the December 2015 MJO episode. This is necessary for two reasons: First, it provides an objective basis for a more direct empirical comparison between the MJO's general structure and the December episode. Second, it ensures that the MJO phase composite can serve to attribute the source of the December 2015 circulation anomalies.

To achieve the aforementioned alignment, corresponding phases of the December 2015 MJO episode and past MJO episodes are subjected to a spatial correlation analysis. If the resulting correlation coefficients at all eight phases for any past episode remains robust above 0.8, that episode is retained. Twenty five out of the 36 past MJO episodes satisfy the criteria and are synthesized to create two MJO phase composites - one for χ_{200} and the other for ψ_{200}.

b. MJO related anomalies

The MJO's contribution to the synoptic conditions that led to the late December 2015 Missouri flooding is calculated by linearly regressing the eight phases of the 2015 December MJO episode on the eight phases of the MJO phase composite. This can be expressed by

$$Y_{(x,y)} = \alpha X_{(x,y)} + b$$

where Y and X are the December MJO episode and the MJO phase composite respectively, both are on a spatial longitude-latitude (lat-lon) domain. The regression coefficient α is considered an estimate of the historical effect of the MJO in December. Therefore $\alpha_{(x,y)}$ is composed of the regression coefficients of several time series regressions at every given grid point within a specified domain. Consider a least-squares regression between two datasets with eight time steps (representative of the MJO phases) over a lat-lon domain (i.e. 180°E-180°W, 40°S-80°N), instead of a regression between two sets of time series. At this point, the statistical estimation of the MJO "component" of the December 2015 circulation anomalies becomes possible by multiplying the regression output $\alpha_{(x,y)}$ to the December MJO episode at every phase. This is done for both χ_{200} and ψ_{200}.

One may argue that a more straightforward calculation of the MJO's contribution to the flooding can be achieved by simply replacing the MJO phase composite with MJO amplitude in the regression. However, MJO amplitude is calculated from the two leading principal components (PCs) generated through EOF analysis ($i.e. amplitude = \sqrt{PC1^2 + PC2^2}$) and therefore, will not include the phase information of the MJO in a regression. While the WH04 RMM indices or PC's of MJO proxies have emerged as the optimal way of explaining MJO variability, unless taken together, a single PC index by itself cannot explain all the variability associated with the MJO. On the other hand, employing the phase composite as used here accounts for both the amplitude of the MJO and its "correct" phase, which is critical in terms of the actual MJO event days. Although somewhat unconventional, our composite approach ensures that both the phasing and amplitude of the MJO are accounted for in the regression.

c. ENSO related anomalies

On the seasonal timescale, the effect of the strong El Niño in December 2015 on circulation is also assessed. The ENSO signal is defined as the Niño 3.4 index (N34), i.e. the normalized SST anomaly over the 5° S - 5° N and 170° W-120° W region of the Pacific Ocean. Here, we use monthly N34 anomalies to approximate the impact of ENSO during each phase of the MJO. For each MJO phase, monthly N34 values are assigned to the 25 previously selected past MJO episodes. The initial outcome is a 25-point index for each MJO phase. However, for the subsequent regression analysis we only use a version of each index with N34 anomalies greater than one standard deviation (i.e. strong ENSO events), which we call a "strong N34 index." While this may appear subjective, it follows previous research that during weak ENSO events, there is no clear Pacific/North American oscillation pattern which prevents influential energy propagation towards the continental U.S. (Huang et al. 1998, Mourtzinis et al. 2016).

To calculate the portion of circulation anomalies attributable to ENSO, ψ_{200} (on a spatial domain) is regressed on the strong N34 index at every phase. The resulting regression outputs are taken as representative of the historic ENSO effect on each MJO phase. We then multiply the regression outputs by values of the N34 index corresponding to the 2015 December MJO episode, to obtain statistical estimates of the December 2015 circulation anomalies attributable to the El Niño by phase.

Once the attributable components of the MJO and ENSO have been calculated for the December MJO episode, a synoptic attribution analysis is carried out. For χ_{200}, we only remove MJO component (i.e. the portion of the circulation anomalies attributable to the MJO) from the December MJO episode. For ψ_{200}, both the MJO and ENSO components (i.e. the typical MJO impact, plus strong ENSO signals regressed out of the 2015 December MJO signal) are removed. What is left, the residual, is then regarded as the portion of the circulation that cannot be explained by ENSO and the MJO.

3. Results and Discussion

Fig. 1 shows the synoptic evolution leading up to the late December 2015 extreme precipitation event and characteristics of the moisture fields associated with it. Precipitation occurred during an extended period (Dec 25-28) over several central U.S. states in a band of thunderstorms generally stretching from Illinois to Texas, with a center over Missouri. Concomitant with this was a quasi-stationary trough over the western U.S., which deepened prior to inducing the strongest precipitation event on December 27. Markedly, the anomalies of vertically integrated moisture flux as shown in Fig. 1 are effective in highlighting the strongest areas of moisture transport associated with the heaviest rainfall, where instability remained strong upstream of the trough along the axis of the mean wind.

To characterize the December 2015 circulation patterns and associated ENSO teleconnection, we first show in Fig. 2a a regression of the Niño 3.4 index on 250-hPa height anomalies from 1950 to 2014, in comparison with the December 2015 circulation anomalies plotted in Fig. 2b. A trans-pacific wave train emanating from Asia into North America is discernable in either case, and depicts an anomalous Aleutian low over the Northern Pacific with a height anomaly of opposite polarity over the Plains states (Chen 2002, Wang et al. 2010).

Next, we illustrate in Fig. 2c the Hovmöller diagram of the 20-year sliding correlation between Niño 3.4 and precipitation averages along a longitudinal cross section of the central U.S. (95°W-85°W;

during December), to depict the link between the changing ENSO teleconnection pattern and local precipitation response. The 20-year sliding window is chosen to examine the decadal-scale variations between ENSO and precipitation (McCabe et al. 1999). There exists an apparent "regime change" in the ENSO-related precipitation anomalies across the target region, from being negatively correlated before 1950 to positively and significantly correlated after 1970. This implies a general amplification effect of the El Niño teleconnection on Southern Plains precipitation as was reported in Bonfils et al. (2015) and Wang et al. (2015). Different sliding windows ranging from 10 to 25 years were also tested. The result (not shown) does not indicate any significant difference in the correlation pattern.

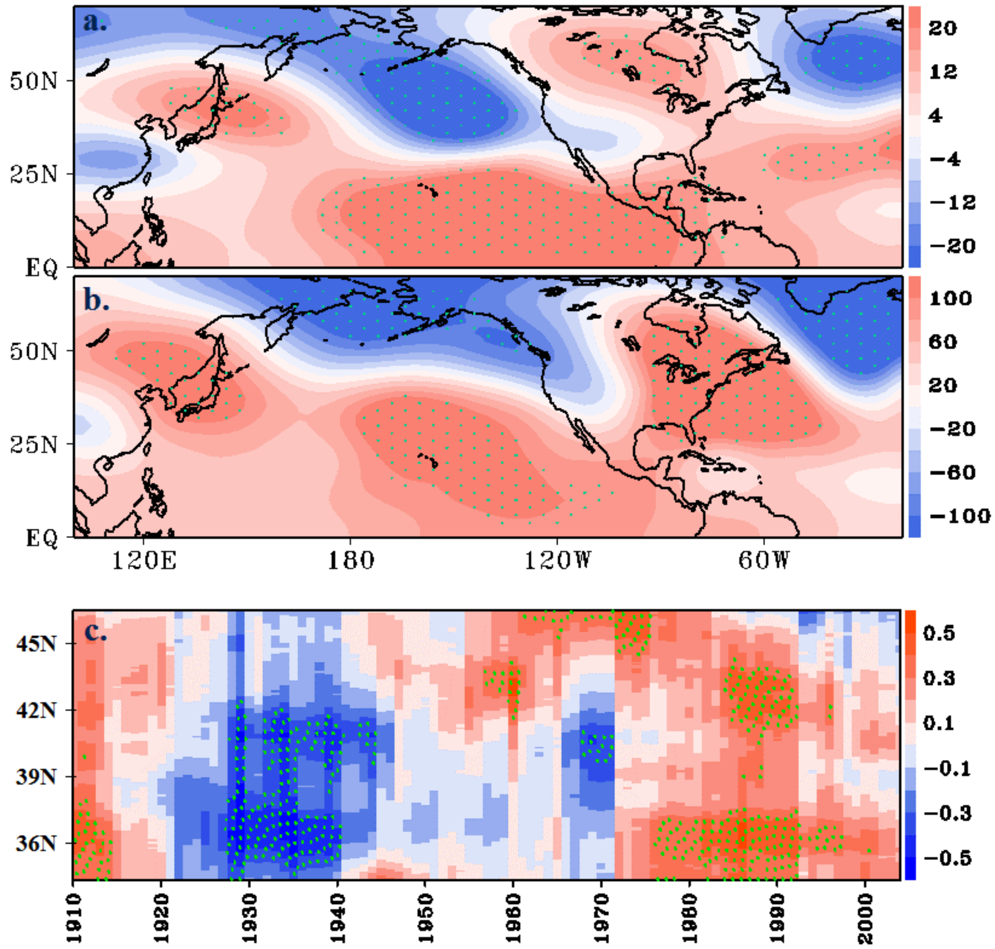

Figure 2
a. Regression of 250-hPa height anomalies with Niño 3.4 in December, from 1950-2014 **b.** December 2015 250 hPa height anomalies as a departure from the 1950-2010 base period. **c.** Latitude-time plot of the 20-years sliding correlation between Nino 3.4 and December precipitation averaged over longitude 95°W-85°W. On the x-axis are the central years of the correlation window. Green stipplings show significant areas at the 95% confidence level.

The MJO episodes embedded in the December 2015 event are also examined. Fig. 3a illustrates the evolution of the global χ_{200} from early December to mid-January, revealing an eastward propagating pattern that shows a clear association with the MJO. As expected, the December MJO episode (Fig. 3a) and the corresponding composite of past MJO cycles (Fig. 3b; created from the alignment method introduced in Section 2.2a) show a coherent eastward propagation. While it may be difficult to differentiate between the two patterns, the residual plot in Fig. 3c, computed by subtracting Fig. 3b from Fig. 3a, does show only regional and somewhat stationary features. This implies that the MJO did have a discernable impact on the global divergent circulation during December 2015. The inadvertent difference in magnitude between the phases of the December MJO episode and that of the composite may be considered a limitation in our regression approach. Although all MJO event days are selected using the same criteria, the magnitude of a well-defined MJO event (amplitude $\geq$ 1 for consecutive pentads and lasts longer than 25 days, Fig. S1b) like the December episode would always be greater than that of any MJO composite. However, a correct phase of the MJO is equally important as its amplitude to North American weather (Yao et al. 2011, Rodney et al. 2013, Johnson et al. 2013) and is a key factor in the context of this study.

One of the fundamental and underlying mechanisms by which tropical convection, such as that associated with the MJO excites Pacific/North American (PNA) like teleconnection patterns (*ref* Fig. 2a) is through the linear dispersion of a Rossby wave triggered by the tropical heating (Johnson et al. 2013). To examine this extratropical wave train induced by the MJO's convective forcing, we repeat the analyses of Fig. 3 using ψ_{200}. This time, we superimpose the wave-activity flux for stationary waves as derived by Takaya and Nakamura 2001 (Fig. 4). The general characteristics of the anomalous circulation patterns between the December 2015 MJO cycle (Fig. 4a) and the composite MJO cycle (Fig. 4b) are similar. Focusing on the period prior to the floods (Phase 6), strong Rossby wave trains steadily propagate eastward from the tropical Pacific towards North America during the preceding weeks (phases 4 and 5; Fig. 4a). The circulation patterns from phases 4 to 6, particularly in phase 6, resemble the ENSO-induced teleconnection pattern; these are consistent with previous findings that MJO-storm track variability associated with ENSO and phases 5 and 6 of MJO have qualitatively similar characteristics to that associated with the PNA (Grise et al. 2013, Goss et al. 2015). Furthermore, Fig. 4a lends support to the notion that it takes a week for any tropical diabatic heating signal to propagate into North America (Lin et al. 2007) and about 2 weeks for the extratropical response to fully develop (Jin and Hoskins 1995). The relatively strong amplitude of the December MJO (*ref* Fig. S1b) forced the eastward flux of Rossby waves which, in turn, triggered robust extratropical atmospheric responses prior to phase 6 (the storm event) as shown by streamfunction and the wave activity flux in Fig. 4.

The residuals in Fig. 4c reflect what is left from the December 2015 cycle after the linear removal of the combined impacts of the MJO and ENSO, as outlined in sections 2.2b and 2.2c. Of the remaining circulation anomalies, the wave-activity flux in Fig. 4c does not resemble any prominent teleconnection source and therefore, mostly comes from internal variability associated with synoptic disturbances over the north Pacific. It is important to mention that, only the removal of strong ENSO events as discussed earlier had a noteworthy impact on the anomalous circulations as seen in Fig. 4c. Yet, ENSO's effect was not as large as the MJO's subseasonal contribution. These results demonstrate that the synoptic patterns associated with the heavy precipitation can be primarily attributed to MJO-related circulation anomalies.

As is shown in Moon et al. (2010) and Roundy et al. (2010), the extratropical response to the MJO is enhanced when MJO-related convection is in phase with heating and convection anomalies associated with certain ENSO phases. However, attempts to uncover a systematic relationship between the MJO and ENSO have yielded conflicting results (Hendon et al. 2007) due to nonlinearity in their combined impact (Roundy et al. 2010). Riddle et al (2013) showed that the occurrence probabilities of Pacific North America (PNA) like MJO teleconnection patterns are more likely to occur during El Niño periods than during La Nina or neutral periods, while a more recent study by Hoell et al. (2014) shows that strong MJO activity significantly weakens the atmospheric branch of ENSO. That said, the simple fact that ENSO imprints are longer than the episodic MJO phases makes attribution difficult. These are the likely reasons why the atmospheric signature of a near historical El Niño was relatively weak in comparison to the MJO during late December 2015.

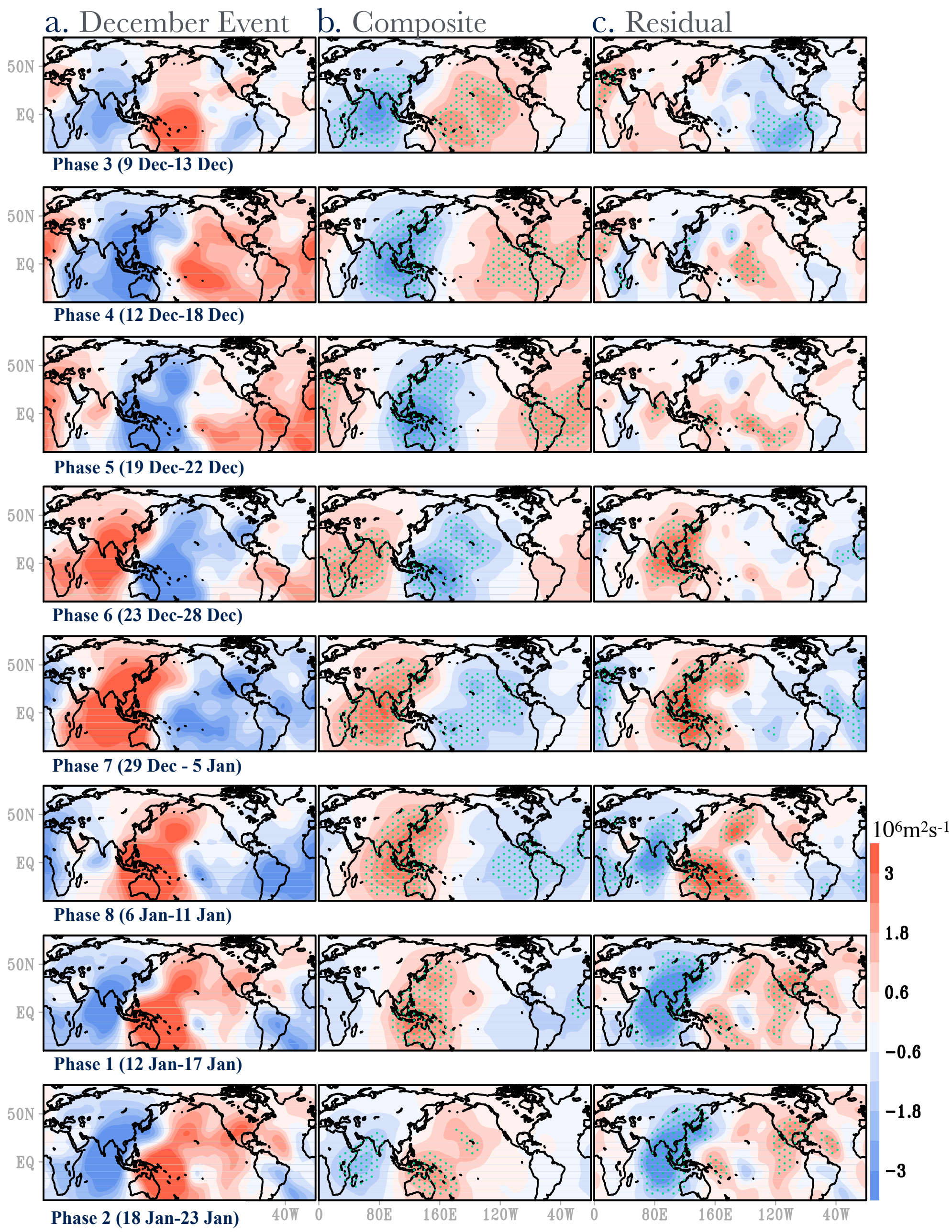

Figure 3
a. 200-hPa velocity potential anomalies based on the eight phases of the December 2015 MJO episode described in the text. **b.** Composite of 200-hPa velocity potential anomalies based on 25 prior MJO episodes **c.** Velocity potential anomalies not linearly explained by the MJO (i.e. linearly regressed construction of the MJO's impact subtracted from the December event anomalies of χ). Green stipplings show significant areas at the 95% confidence level.

265

266

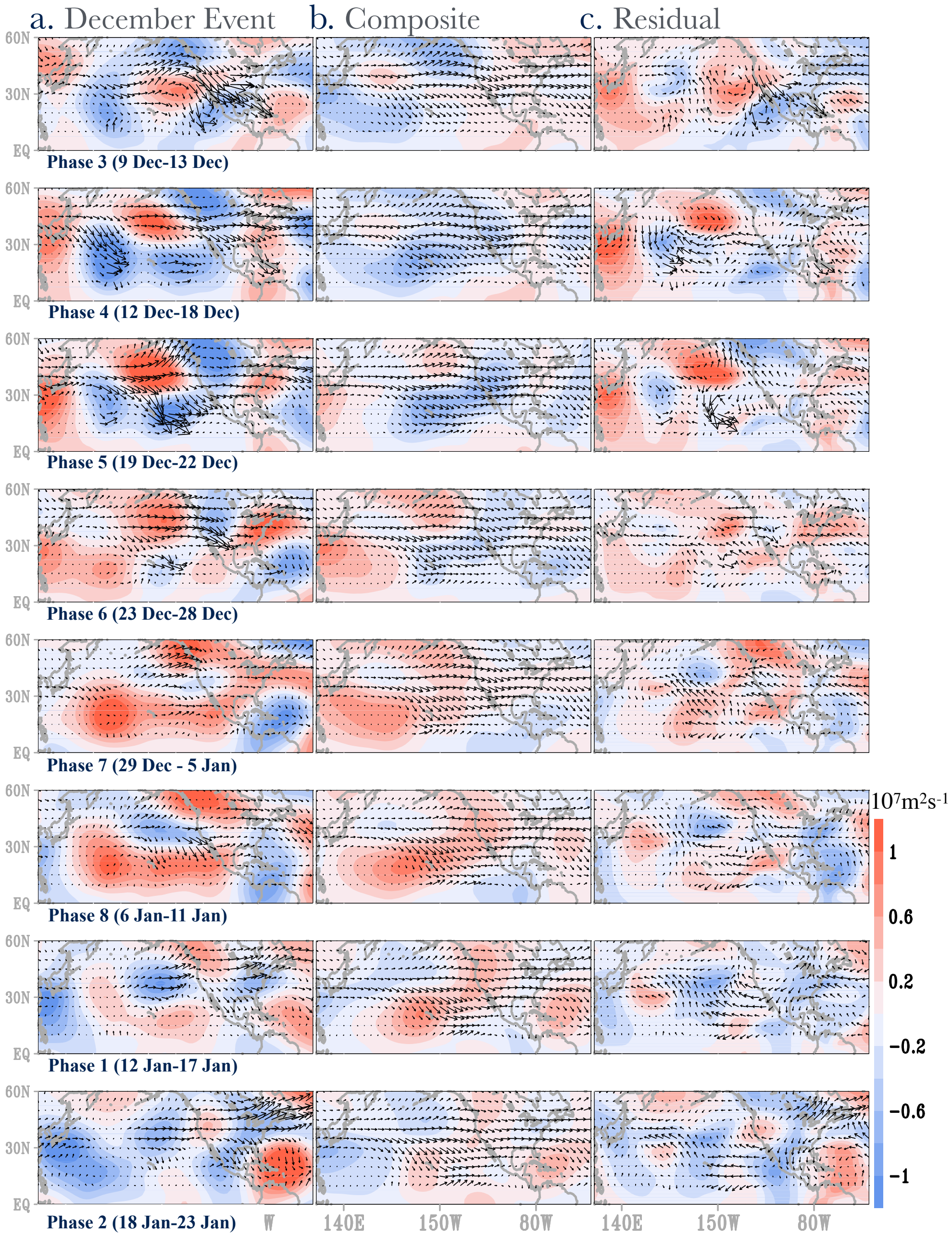

Figure 4

a. 200-hPa streamfunction anomalies based on the eight phases of the December 2015 MJO episode described in the text. **b.** Composite of 200-hPa streamfunction anomalies based on 25 prior MJO episodes **c.** Streamfunction anomalies not linearly explained by the MJO and ENSO (i.e. linearly regressed constructed impact of both the MJO and ENSO subtracted from the December event anomalies of Ψ). Corresponding wave-activity fluxes are superimposed in vectors.

b. Climate change impacts

Recall that Fig. 2c depicts a regime change in the ENSO-related precipitation anomalies across several parts of the Central and Southern Plains. To attribute the causes of this apparent regime change, we repeat the analysis in Fig. 2c using two forcing scenarios of 17 CMIP5 models. The result is presented in Fig. 5 - the CMIP5 representation of the 20-years sliding correlation between the Nino-3.4 index and precipitation. In the GHG run (Fig. 5a), the model spread (contours), along with the ensemble mean (shading), which is the composite mean of 17 models (table 1), depict a general strengthening of the relationship between ENSO and precipitation across the central U.S. Note that

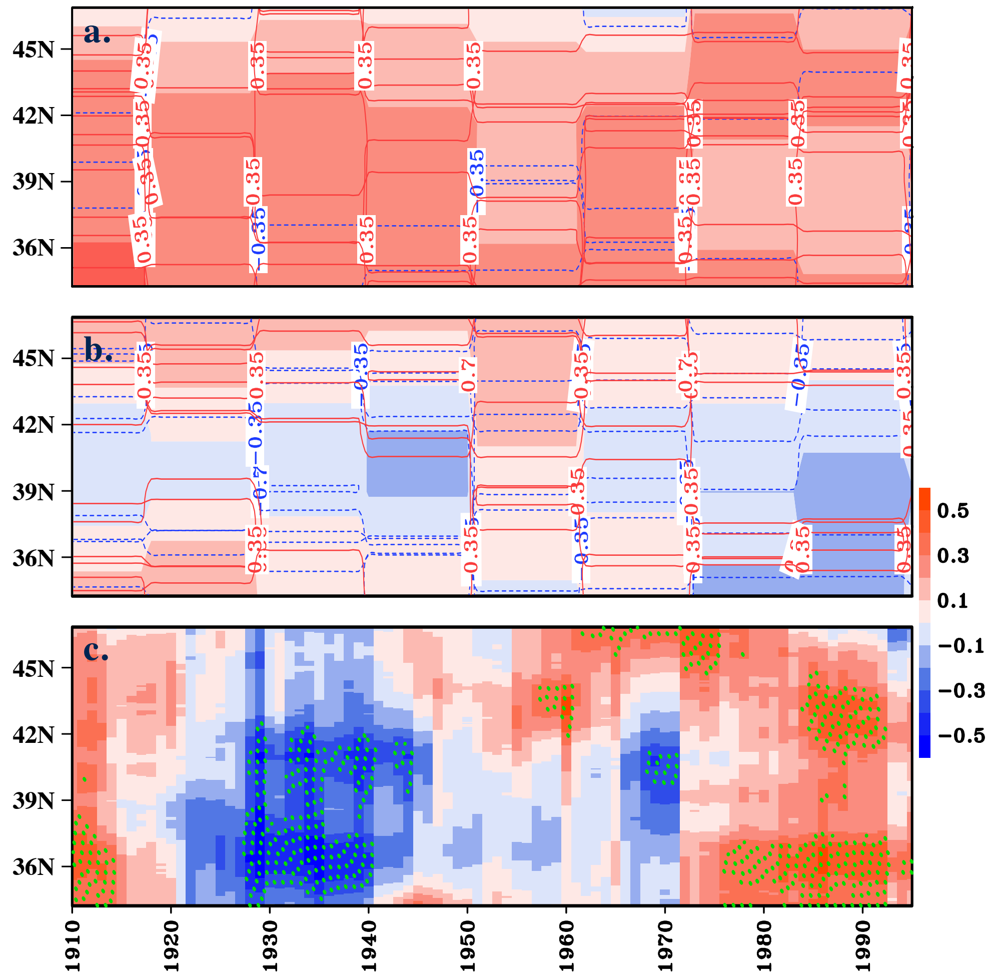

Figure 5
20-years sliding correlation between the December Nino 3.4 index and precipitation averaged longitudinally over 95°W-85°W, as depicted by 17 CMIP5 models in two scenarios - (a) GHG run and (b) Natural run. Shading represents the ensemble mean. Years on the *x* axis represent the central years of the sliding window. The ensemble spread is in contours and only statistically significant contours based on the Student's t-test at the 95% confidence level are drawn. Fig. 5c is a repeat of Fig. 2c with a comparable timespan to the model runs.

only statistically significant contours based on the Student's t-test at the 95% confidence level are drawn. On the contrary, the NAT run (Fig. 5b) exhibits a relatively weak relationship between ENSO and precipitation. Although this result does not directly address the impact of climate change specifically on the December 2015 Missouri flooding, it does lend support to the observations (Fig. 5c) and previous studies (e.g., Wang et al. 2015) that the regime change in the ENSO-induced precipitation anomalies across the Southern Plains is likely linked to the warming climate. Further examination of the MJO's effect on precipitation in the Southern Plains will be needed when the CMIP5 models' performance in the tropical intraseasonal variability is improved.

4. Concluding remarks

The spatial and temporal features of the large-scale circulation anomalies associated with the late-December 2015 flood in Missouri were analyzed. Through synoptic attribution analyses, we found an interference between certain MJO phases and the El Niño during the time leading up to the Missouri flood. Consequently, an unusually high precipitation event occurred during phase 6 of the MJO cycle, i.e. from 23 to 28 December. At this time, the MJO's convection amplified a trans-Pacific Rossby wave train that resembles the ENSO-driven teleconnection pattern from the tropics to form the constructive interference. This contributed to an energized upper-level circulation and strong jet stream flow over the contiguous United States and led to the advection of intense cyclone activity into the Central and Southern Plains (e.g. Bell et al. 1995). In the long term, the effect of anthropogenic warming on the December event is also implied through the analysis of several CMIP5 models. The models suggest that the response of precipitation in the central U.S. to ENSO would be enhanced owing to a warming climate. With this study, we seek to provide a meaningful contribution to the literature on the synoptic attribution of climate extremes.

a.

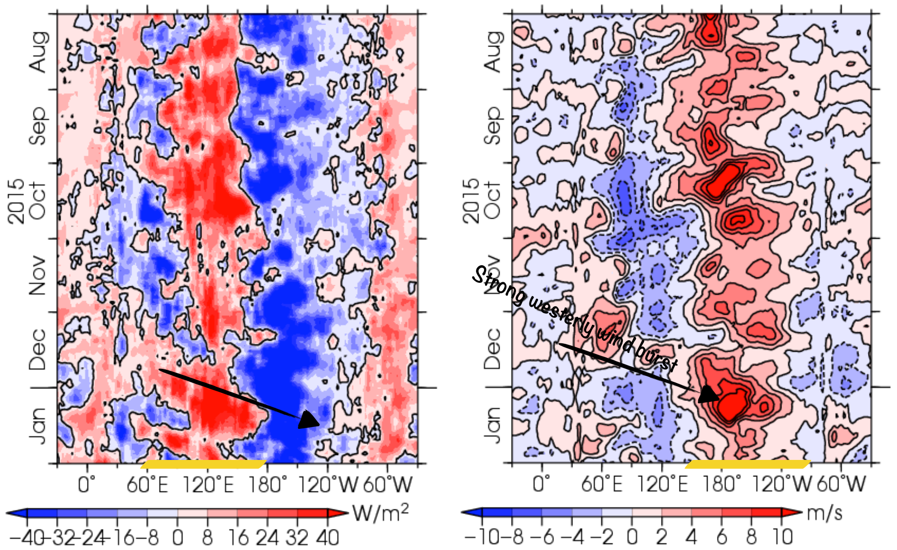

b.

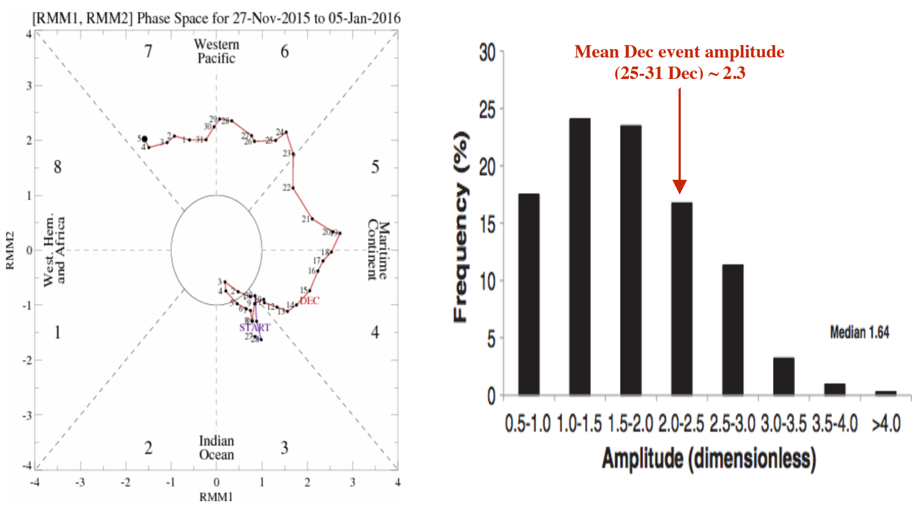

Supplementary Figure 1 (Figure S1)

Longitude-time plot of the 7-day mean **a.** outgoing longwave radiation (OLR) and 850 mb wind anomalies (base period: 1981-2010) averaged over 5S-5N, from July-Dec 2015. The thick yellow bars on the longitudinal axes highlight the ENSO region. (*figures courtesy of the Tokyo Climate Centre*). **b.** Phase space diagram for 27Nov2015 - 5Jan2016 illustrating the phase and amplitude of the activity days of the 2015 MJO cycle, based on the principal components (RMM) of the first two EOFs from a combined EOF analysis using 850 hPa zonal wind, 200 hPa zonal wind and OLR. Counter-clockwise movement around the diagram indicates an eastward propagating signal across eight phases from the Indian Ocean to the Pacific and later the western hemisphere. Color of lines distinguish different months and dates are annotated. The farther away from the center of the circle the stronger the MJO signal (*figure courtesy of the Climate Prediction Center*) ; and frequency distribution of MJO amplitudes during extended boreal winters (1 Nov–31 Mar, 1979–2010). Median value: 1.64. (*figures adopted from Jones and Carvalho 2014*)

Acronym	**Model full name**	**Center/Institute, country**	**Resolution (lon.xlat.)**	**Ensemble size (max)**
BCC-CSM1	Beijing Climate Center, Climate System Model, version 1.1	Beijing Climate Center, Meteorological Administration, China	2.8° x 2.8°	1
BNU-ESM	Beijing Normal University—Earth System Model	College of Global Change and Earth System Science (GCESS), China	2.8° x 2.8°	1
CanESM2	Canadian Earth System Model, version 2	Canadian Center for Climate Modeling and Analysis, Canada	2.8° x 2.8°	5
CCSM4	Community Climate System Model, version 4	National Center for Atmospheric Research, USA	1.25°x1.0°	5
CNRM-CM5	Centre National de Recherches Météorologiques Coupled Global Climate Model, version 5	National Centre for Meteorological Research, France	1.4° x 1.4°	10
CSIRO-Mk3	Commonwealth Scientific and Industrial Research Organisation Mark, version 3.6.0	Commonwealth Scientific and Industrial Research Organization/ Queensland Climate Change Centre of	1.8° x 1.8°	10
FGOALS-g2	Flexible Global Ocean-Atmosphere-Land System Model, grid point version 2	LASG, Institute of Atmospheric Physics, Chinese Academy of Sciences, China	2.8° x 1.6°	4
GFDL-CM3	Geophysical Fluid Dynamics Laboratory Climate Model version 3	NOAA Geophysical Fluid Dynamics Laboratory, USA	2.5° x 2.0°	5
GFDL-ESM2	Geophysical Fluid Dynamics Laboratory Earth Science Model 2 with Modular Ocean Model (MOM), version 4.1	NOAA Geophysical Fluid Dynamics Laboratory, USA	2.5° x 2.0°	3
GISS-E2-H	Goddard Institute for Space Studies Atmospheric Model E, version 2, coupled with the Hybrid Coordinate Ocean Model	NASA Goddard Institute for Space Studies, USA	2.5° x 2.0°	5
GISS-E2-R	Goddard Institute for Space Studies Model E, version 2, coupled with Russell ocean model	NASA Goddard Institute for Space Studies, USA	2.5° x 2.0°	5
HadGEM2-ES	Hadley Centre Global Environmental Model 2, Earth System	Met Office Hadley Centre, UK	1.8° x 1.25°	4
IPSL-CM5A-MR	L'Institut Pierre-Simon Laplace Coupled Model, version 5A, medium resolution	Institute Pierre Simon Laplace, France	2.5° x 1.25°	1
MIROC-ESM-CHEM	Model for Interdisciplinary Research on Climate Earth System Model, chemistry coupled version	Japan Agency for Marine-Earth Science and Technology, Atmosphere and Ocean Research Institute (The	2.8° x 2.8°	3
MIROC-ESM	Model for Interdisciplinary Research on Climate Earth System Model	Japan Agency for Marine-Earth Science and Technology, Atmosphere and Ocean Research Institute, and National	2.8° x 2.8°	3
MRI-CGCM3	Meteorological Research Institute Coupled General Circulation Model, version 3	Meteorological Research Institute, Japan	1.1° x 1.1°	3
NorESM1-M	Norwegian Earth System Model, version 1, intermediate resolution	Norwegian Climate Center, Norway	2.5° x 1.9°	3

Supplementary Table 1 (Table S1)

Full name, institute, ensemble size, and spatial resolution of the CMIP5 models

References

1. Bonfils CJW, Santer BD, Phillips TJ, Marvel K, L. R. Leung, C. Doutriaux, A. Capotondi (2015) Relative Contributions of Mean-State Shifts and ENSO-Driven Variability to Precipitation Changes in a Warming Climate. J. Climate, 28, 9997–10013
2. Bell GD, Janowiak JE (1995) Atmospheric Circulation Associated with the Midwest Floods of 1993. *Bull. Am.*

Meteorol. Soc., 76, 681–695

3. Chen T (2002) A North Pacific Short-Wave Train during the Extreme Phases of ENSO. *J. Climate,* 15, 2359–2376.
4. Daly C, Halbleib M, Smith JI, Gibson WP, Doggett MK, Taylor GH, Curtis J, Pasteris PA (2008) Physiographically-sensitive mapping of temperature and precipitation across the conterminous United States. International Journal of Climatology, 28: 2031-2064
5. Fan Y, van den Dool H (2004) Climate Prediction Center global monthly soil moisture data set at 0.5° resolution for 1948 to present, J. Geophys. Res., 109, D10102
6. Grise KM, Son S-W, Gyakum JR (2013) Intraseasonal and Interannual Variability in North American Storm Tracks and Its Relationship to Equatorial Pacific Variability. *Mon. Weather Rev.*, 141, 3610–3625
7. Hendon HH, Wheeler MC, Zhang C (2007) Seasonal Dependence of the MJO–ENSO Relationship. *J. Climate,* 20, 531–543
8. Higgins RW, Schemm JKE, Shi W, Leetmaa A (2000) Extreme precipitation events in the Western United States related to tropical forcing. *J. Clim.*, 13, 793–820
9. Hirschboeck KK (1991) Climates and floods. National water summary 1988-89 Floods and droughts: Hydrologic perspectives on water issues, R. W. Paulson et al., Eds., USGS Water-Supply Paper 2375, 67–88. [Available online at http:// pubs.usgs.gov/wsp/2375/report.pdf.]
10. Hoell A, Barlow M, Wheeler MC, Funk C (2014) Disruptions of El Niño–Southern Oscillation Teleconnections by the Madden–Julian Oscillation, Geophys. Res. Lett., 41, 998–1004
11. Holmes RR, Watson KM, Harris TE (2016) Preliminary peak stage and streamflow data at selected U.S. Geological Survey streamgages for flooding in the central and southeastern United States during December 2015 and January 2016: U.S. Geological Survey Open-File Report 2016–1092, 27 p
12. Jin F, Hoskins BJ (1995) The direct response to tropical heating in a baroclinic atmosphere. J. Atmos. Sci., 52, 307–319
13. Johnson RH, Ciesielski PE (2013) Structure and Properties of Madden–Julian Oscillations Deduced from DYNAMO Sounding Arrays. J. Atmos. Sci., 70, 3157–3179
14. Jones C, Carvalho LMV (2014) Sensitivity to Madden–Julian oscillation variations on heavy precipitation over the contiguous United States. Atmos. Res., 147–148, 10–26
15. Joyce RJ, Janowiak JE, Arkin PA, Xie P (2004) CMORPH: A method that produces global precipitation estimates from passive microwave and infrared data at high spatial and temporal resolution. J. Hydrometeor., 5, 487–503
16. Kalnay E and coauthors (1996) The NCEP/NCAR 40- year reanalysis project. Bull. Amer. Meteor. Soc., 77, 437–471
17. Kiladis GN, Dias J, Straub KH, Wheeler MC, Tulich SN, Kikuchi K, Weickmann KM, and Ventrice MJ (2014) A comparison of OLR and circulation-based indices for tracking the MJO. Mon. Wea. Rev., 142, 1697–1715.
18. Lin H, Brunet G, Derome J (2007) The nonlinear transient atmospheric response to tropical forcing. J. Climate, 20, 5642–5665
19. McCabe GJ and Dettinger MD (1999) Decadal variations in the strength of ENSO teleconnections with precipitation in the western United States. Int. J. Climatol. 19: 1399–1410
20. Meehl GA, Tebaldi C, Teng H, Peterson TC (2007) Current and future U.S. weather extremes and El Niño. Geophysical Research Letters, 34, L20704
21. Moon JY, Wang B, Ha KJ (2012) MJO Modulation on 2009/10 winter snowstorms in the United States. *J. Clim.*, 25, 978–991

22. Mourtzinis S, Ortiz BV, Damiandis D (2016) Climate Change and ENSO Effects on Southeastern US Climate Patterns and Maize Yield. Sci. Rep. 6, 29777
23. Riddle EE, Stoner MB, Johnson NC, L'Heureux ML, Collins DC, Feldstein SB (2013) The impact of the MJO on clusters of wintertime circulation anomalies over the North American region. *Clim. Dyn.*, 40, 1749–1766
24. Rodney M, Lin H, Derome J (2013) Subseasonal Prediction of Wintertime North American Surface Air Temperature during Strong MJO Events. *Mon. Weather Rev.*, 141, 2897–2909
25. Roundy PE, MacRitchie K, Asuma J, Melino T (2010) Modulation of the global atmospheric circulation by combined activity in the Madden–Julian Oscillation and the El Nin˜o-Southern Oscillation during Boreal winter. J Clim 23:4045–4059
26. Schubert SD, Chang Y, Suarez MJ, Pegion PJ (2008) ENSO and wintertime extreme precipitation events over the contiguous United States. *J. Clim.*, 21, 22–39
27. Stevenson S, Fox-Kemper B, Jochum M, Neale R, Deser C, Meehl G (2012) Will There Be a Significant Change to El Niño in the Twenty-First Century?. J. Climate, 25, 2129–2145
28. Takaya K, Nakamura H (2001) A Formulation of a Phase-Independent Wave-Activity Flux for Stationary and Migratory Quasigeostrophic Eddies on a Zonally Varying Basic Flow. *J. Atmos. Sci.*, 58, 608–627
29. Taylor KE, Stouffer RJ, Meehl GA (2012) An overview of CMIP5 and the experiment design. Bull. Amer. Meteor. Soc., 93, 485–498
30. Ventrice MJ, Wheeler MC, Hendon HH, Schreck CJ, Thorncroft CD, and Kiladis GN (2013) A Modified Multivariate Madden–Julian Oscillation Index Using Velocity Potential. Mon. Wea. Rev., 141, 4197–4210
31. Wang S-Y, Huang W-R, Hsu H-H, Gillies RR (2015) Role of the strengthened El Niño teleconnection in the May 2015 floods over the southern Great Plains, Geophys. Res. Lett., 42, 8140–8146
32. Wheeler MC, Hendon HH (2004) An All-Season Real-Time Multivariate MJO Index: Development of an Index for Monitoring and Prediction. *Mon. Weather Rev.*, 132, 1917–1932
33. Yao Wenqing, Hai Lin and Jacques Derome (2011) Submonthly Forecasting of Winter Surface Air Temperature in North America Based on Organized Tropical Convection, Atmosphere-Ocean, 49:1, 51-60
34. Zhang C (2013) Madden-julian oscillation: Bridging weather and climate. *Bull. Am. Meteorol. Soc.*, 94, 1849–1870
35. Zhou S, L'Heureux M, Weaver S, Kumar A (2012) A composite study of the MJO influence on the surface air temperature and precipitation over the Continental United States. *Clim. Dyn.*, 38, 1459–1471